



Cite as  
Nano-Micro Lett.  
(2021) 13:163

## Advances and Challenges in Two-Dimensional Organic–Inorganic Hybrid Perovskites Toward High-Performance Light-Emitting Diodes

Miao Ren<sup>1</sup>, Sheng Cao<sup>1</sup>, Jialong Zhao<sup>1</sup>, Bingsuo Zou<sup>1</sup>, Ruosheng Zeng<sup>1</sup> ✉

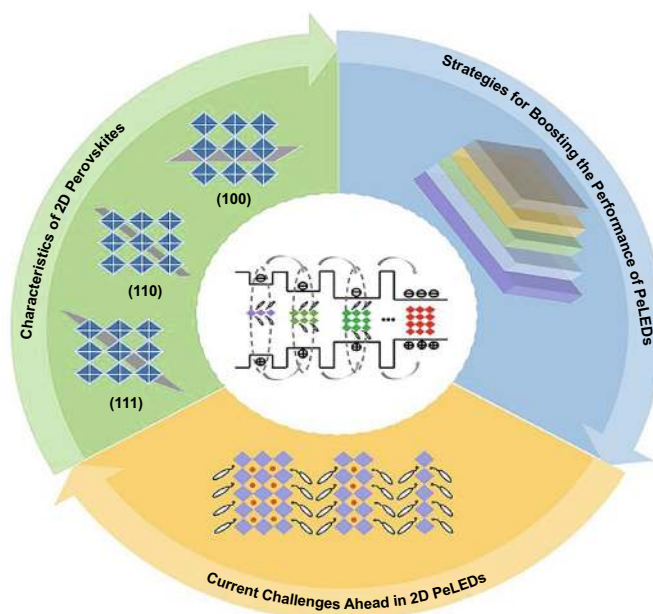
Received: 20 April 2021  
Accepted: 18 June 2021  
Published online: 2 August 2021  
© The Author(s) 2021

### HIGHLIGHTS

- The fundamental structure, photophysical and electrical properties of 2D perovskite films were illustrated systematically.
- The advantages and challenges of 2D perovskite light-emitting diodes (PeLED) have been also discussed, which may benefit the audience to get insight into the 2D perovskite materials as well as the resultant LED devices.
- An outlook on further improving the efficiency of pure-blue PeLEDs, enhancing the operational stability of PeLEDs and reducing the toxicity to push this field forward was also provided.

**ABSTRACT** Two-dimensional (2D) perovskites are known as one of the most promising luminescent materials due to their structural diversity and outstanding optoelectronic properties. Compared with 3D perovskites, 2D perovskites have natural quantum well structures, large exciton binding energy ( $E_b$ ) and outstanding thermal stability, which shows great potential in the next-generation displays and solid-state lighting. In this review, the fundamental structure, photophysical and electrical properties of 2D perovskite films were illustrated systematically. Based on the advantages of 2D perovskites, such as special energy funnel process, ultra-fast energy transfer, dense film and low efficiency roll-off, the remarkable achievements of 2D perovskite light-emitting diodes (PeLEDs) are summarized, and exciting challenges of 2D perovskite are also discussed. An outlook on further improving the efficiency of pure-blue PeLEDs, enhancing the operational stability of PeLEDs and reducing the toxicity to push this field forward was also provided. This review provides an overview of the recent developments of 2D perovskite materials and LED applications, and outlining challenges for achieving the high-performance devices.

**KEYWORDS** Two-dimension; Perovskite; Light-emitting diodes; Optical properties



✉ Ruosheng Zeng, [zengrsh@guet.edu.cn](mailto:zengrsh@guet.edu.cn)

<sup>1</sup> School of Physical Science and Technology, MOE Key Laboratory of New Processing Technology for Non-Ferrous Metals and Materials, Guangxi Key Laboratory of Processing for Non-Ferrous Metals and Featured Materials, Guangxi University, Nanning 530004, People's Republic of China



## 1 Introduction

Perovskite materials have attracted extensive attention due to their interesting properties such as photoluminescence, electroluminescence, high carrier mobility, large optical absorption coefficient and good nonlinear optical properties [1–10]. The chemical composition of traditional perovskite is  $\text{CaTiO}_3$ , which belongs to orthorhombic system. The origin of perovskite dates back to 1839 when Gustav Rose, a German mineralogist, discovered perovskite rock samples in the Ural Mountains and named after L. A. Perovski, a Russian geologist. After that, materials with similar structure to  $\text{CaTiO}_3$  are called perovskite. The formula of three-dimensional (3D) halide perovskite is  $\text{ABX}_3$  ( $A = \text{MA}^+, \text{FA}^+, \text{Cs}^+, \text{Rb}^+, \text{K}^+$ ;  $B = \text{Pb}^{2+}, \text{Cu}^{2+}, \text{Sn}^{2+}$ ;  $X = \text{Cl}^-, \text{Br}^-, \text{I}^-$ ) [11–21].

The preparation of  $\text{CsPbX}_3$  was successfully reported in 1893 [22]. However, it was not until the 1950s that perovskite crystal structure and properties were discovered. In 1978, the crystal structure and properties of  $\text{MAPbX}_3$  were synthesized and determined by Weber et al. [23]. Subsequently, Mitzi et al. further studied the unique optoelectronic properties of three-dimensional (3D) perovskites [24, 25]. However, until 2009, perovskite materials broadly attracted researchers' interest. Miyasaka reported for the first time that  $\text{MAPbBr}_3$  and  $\text{MAPbI}_3$  sensitized  $\text{TiO}_2$  to achieve visible light conversion in photoelectrochemical cells [26]. Beyond solar cells, perovskite materials were also used in LEDs. In 2014, Tan et al. [27] realized near-infrared, green and red room temperature electroluminescence by adjusting the halide compositions in perovskites, which used 3D methylammonium lead halide perovskites as the emissive layer. However, the focus has gradually shifted to low-dimensional perovskite films. Different from three-dimensional perovskites, there is at least one large organic cation in the low-dimensional perovskites, which cannot match the cubic center. Interestingly, 3D, 2D, 1D and 0D perovskites can be formed by different bonding methods of octahedral  $[\text{BX}_6]^{4-}$ . At the same time, 2D perovskite materials have unique physical and chemical properties due to the influences of quantum confinement and dielectric confinement effect [28]. In addition, the existence of organic cations greatly improves the stability of perovskites [29]. Therefore, 2D perovskites have become star materials used in many fields, including LEDs [30, 31], solar cells [32–35], photodetectors [36, 37], lasers [38, 39] and sensors [40].

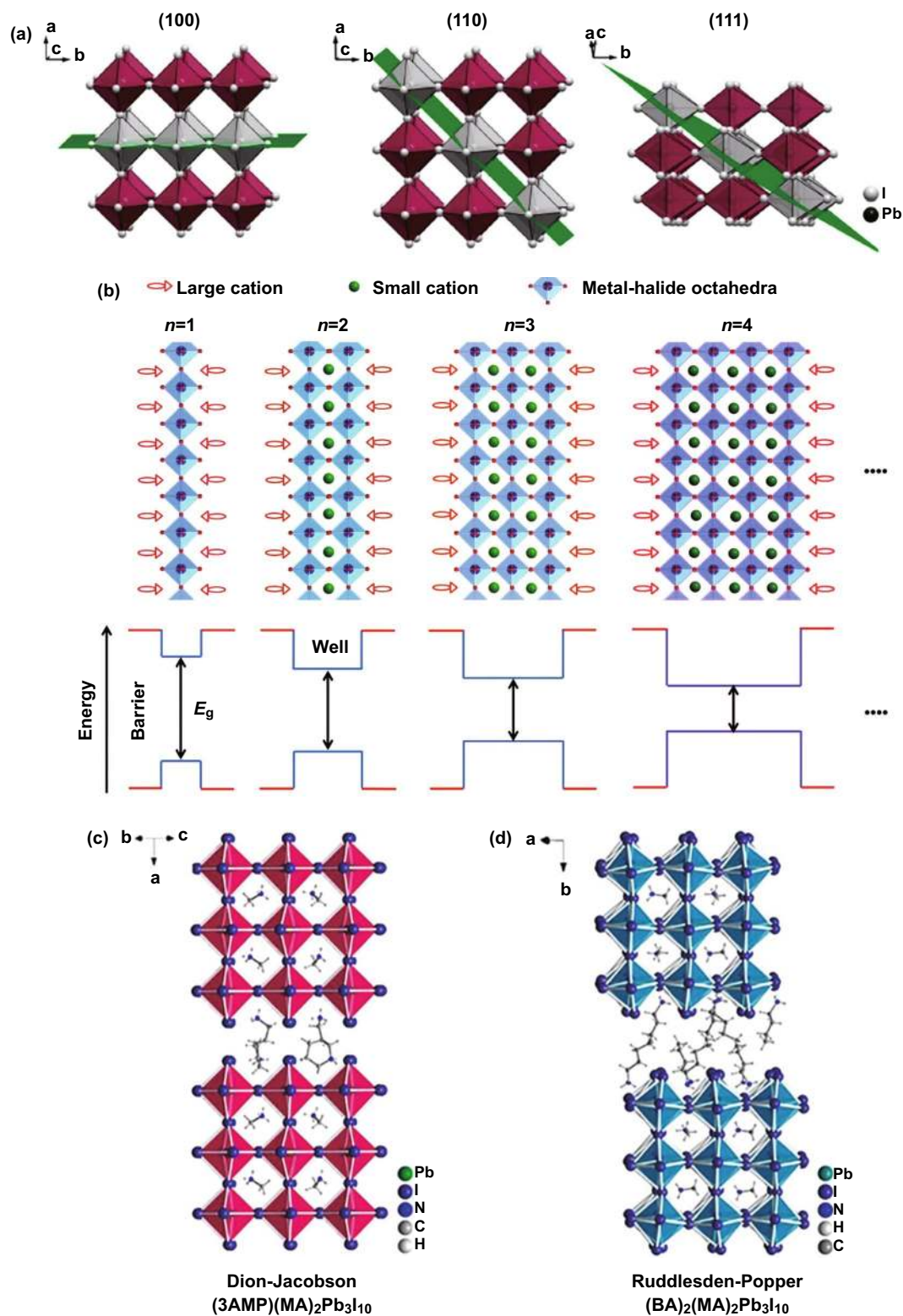
In the early stage, the LEDs with 2D perovskites as the emissive layer can only observe the electroluminescence at low temperature. In recent years, a quasi-2D perovskite structure has been proposed by introducing organic cations into 3D perovskites, which can assemble multiple quantum wells. The existence of quantum wells not only benefits the formation of exciton, but also increases the difficulty of exciton separation. This makes quasi-2D perovskite materials promising for high-performance LEDs. Sargent et al. [41] realized the photoexcitation funneling to the lowest band-gap emitter in the mixture by dimensional modulation. In 2016, Huang et al. [42] reported a multi quantum well-based PeLED, showing a very high external quantum efficiency (EQE) of 11.7%. Recently, Lee et al. [43] prepared high-quality quasi-2D perovskite films by a simple and novel encapsulation growth method and obtained high-efficiency sky-blue LEDs with maximum EQE of 12.8%. Di et al. [44] reported near-infrared LEDs with quasi-2D and 3D perovskites and insulating polymers as emissive layers. The EQE was as high as 20.1%. Su et al. [45] proposed a co-interlayer engineering strategy for the preparation of quasi-2D perovskite materials, which makes the green LEDs have a high current efficiency of  $66.1 \text{ cd A}^{-1}$ .

In this review, the structural types of 2D perovskite are reviewed. Then, the unique optical properties of 2D perovskite are discussed as the advantages of the emitting layer of LEDs. In addition, the effects of different types of organic cations on devices and the design principles of high-efficiency 2D PeLEDs are summarized. Finally, we emphasize that 2D PeLEDs have great potential in the fields of display and solid-state lightings.

## 2 Characteristics of 2D Perovskite Materials

### 2.1 Structure of 2D Perovskite Materials

2D perovskite materials with (100)-oriented, (110)-oriented and (111)-oriented structures are formed by cutting along the specific (hkl) planes of the corresponding 3D perovskite structures (Fig. 1a) [46–48]. The most studied are the (100)-oriented 2D perovskites with  $\text{K}_2\text{NiF}_4$  or  $\text{RbAlF}_4$  crystal structure, and the general formula is  $\text{A}'_2\text{A}_{n-1}\text{B}_n\text{X}_{3n+1}$ . The general formula of (110)-oriented 2D perovskite is  $\text{A}'_2\text{A}_m\text{B}_m\text{X}_{3m+2}$ . Because octahedrons are usually highly distorted, there will be many interesting physical phenomena



**Fig. 1** a Schematic diagram of 2D perovskite series with different orientations. Copyright 2018 American Chemical Society [47]. b Schematic diagram of quantum wells perovskites. Copyright 2020 Wiley-Blackwell [65]. Comparison between c Dion–Jacobson phase and d Ruddlesden–Popper phase for halide perovskite. 3AMP = 3-(aminomethyl)piperidinium, 4AMP = 4-(aminomethyl)piperidinium, MA = methylammonium, BA = butylammonium. Copyright 2018 American Chemical Society [50]

at room temperature, such as self-trapping exciton and white light emission [49]. The general formula of (111)-oriented 2D perovskite is  $A'_2A_{q-1}B_qX_{3q+3}$  ( $q > 1$ ).

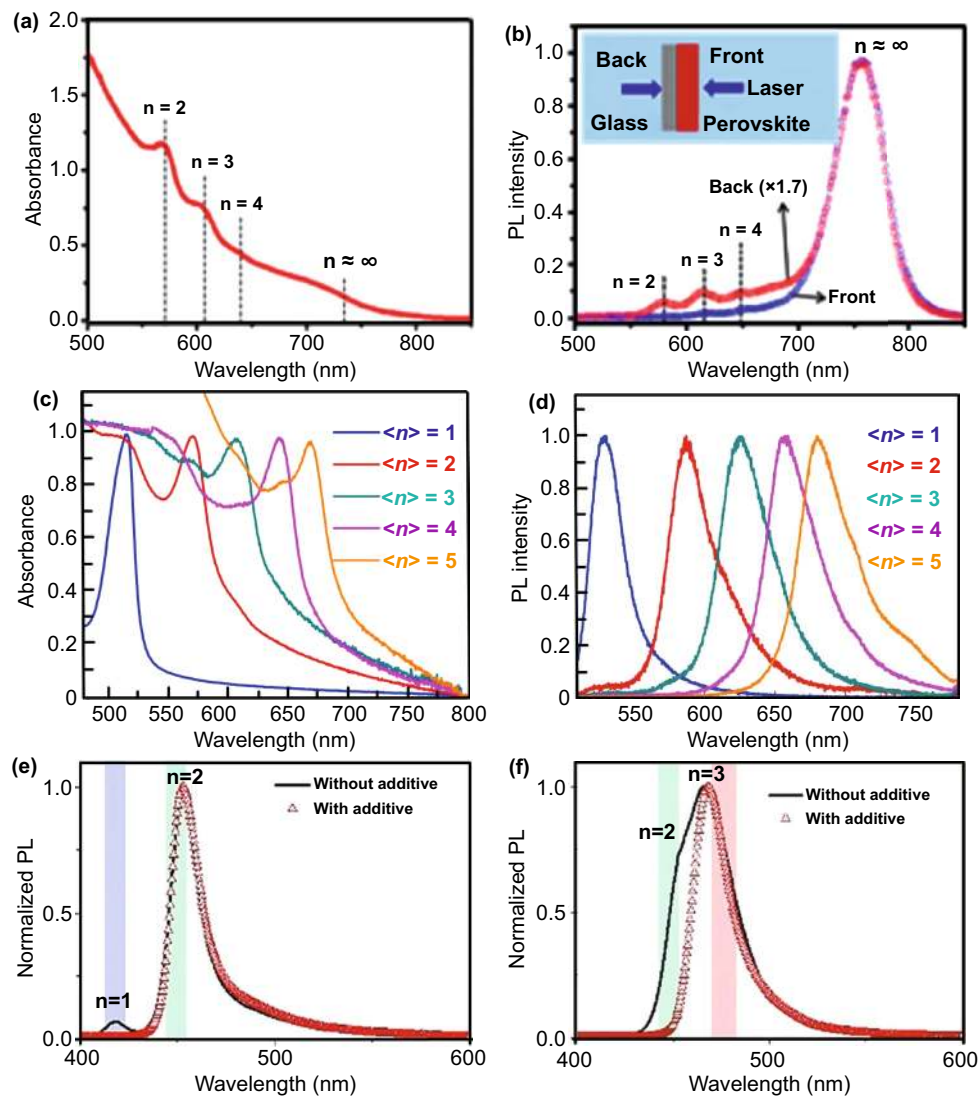
At present, (100)-oriented perovskites are the most widely studied 2D perovskites, which can be further divided into Ruddlesden–Popper (RP) and Dion–Jacobson (DJ) phases. The general formulas of RP and DJ perovskites are  $A'_2A_{n-1}B_nX_{3n+1}$  and  $A''A_{n-1}B_nX_{3n+1}$ , respectively, where  $A'$  represents a large aromatic or aliphatic alkyl ammonium cation (monovalent) and  $A''$  is divalent cation.  $A$  is a small cation like  $\text{CH}_3\text{NH}_3^+$ ,  $\text{Cs}^+$ ,  $\text{CH}(\text{NH}_2)_2^+$ ,  $B$  refers to a divalent metal cation ( $\text{Pb}^{2+}$ ,  $\text{Sn}^{2+}$ ,  $\text{Cu}^{2+}$ ,  $\text{Cd}^{2+}$ ,  $\text{Zn}^{2+}$ ), and  $X$  represents an anion, such as  $\text{Cl}^-$ ,  $\text{Br}^-$ ,  $\text{I}^-$ ,  $\text{SCN}^-$  and  $\text{F}^-$ . For the DJ phase  $(3\text{AMP})(\text{MA})_2\text{Pb}_3\text{I}_{10}$ , the layers overlap completely without any displacement (Fig. 1c) [50]. Different from DJ phase, the layers of  $(\text{BA})_2(\text{MA})_2\text{Pb}_3\text{I}_{10}$  show (1/2, 1/2) displacement in RP phase (Fig. 1d) [51]. In addition, the interlayer distance between DJ and RP phase is quite different. Generally, the interlayer distance of RP phase is larger than that of DJ phase. RP phase has double-layer organic cations, which increases the interlayer distance.

The (110)-oriented structures are the most distorted and uncommon, and few cations can stabilize them. Generally, these cations have small ionic radii and highly symmetrical structures [52]. The (100)-oriented 2D perovskites consist of flat perovskite sheets, while the (110)-oriented perovskites have corrugated layers. The structures can be defined as  $2 \times 2$ ,  $3 \times 3$ ,  $4 \times 4$ , etc., according to the corrugation length. These perovskites with roof shape are named “ $n \times n$ ,” where  $n$  is the number of octahedrons that make up half of the roof.

Different from other layered perovskites, (111)-oriented perovskites are actually a kind of defective perovskites. The formation of layered perovskites is due to the introduction of vacancies rather than large organic cations. The (111)-oriented perovskites belong to M-site-deficient, and the general formula is  $A'_2A_{q-1}B_qX_{3q+3}$  ( $q > 1$ ). The (111)-oriented perovskites can be obtained by cutting along the volume diagonal of 3D perovskite cell, which selectively “eliminates” the metal sites in the cutting process. Thus, if the B site contains only divalent metal ions, there is no way to form (111)-oriented perovskites. When B site is the same metal ion ( $q = 2$ ), some common (111)-oriented perovskite materials such as  $\text{FA}_3\text{Bi}_2\text{Br}_9$  [53],  $\text{Cs}_3\text{Bi}_2\text{Br}_9$  [54],  $\text{Cs}_3\text{Sb}_2\text{I}_9$  [55],  $\text{Rb}_3\text{Sb}_2\text{I}_9$  [56] and  $\text{MA}_3\text{Bi}_2\text{I}_9$  [57].

## 2.2 $n$ Values in the 2D Perovskites

The value of  $n$  in the formula is defined as the number of  $[\text{BX}_6]^{4-}$  octahedral layers, which can be achieved by adjusting the stoichiometry of the precursor solution. The band gap, carrier mobility and  $E_b$  of 2D perovskite are all related to  $n$  value. At present, in most reports, researchers have assumed that there is a specific  $n$  value in 2D perovskite thin films. However, the 2D perovskites prepared according to the formula are usually mixtures with different  $n$  values, even though the purpose is to prepare pure 2D perovskites [58]. Jin et al. prepared 2D perovskite  $(\text{BA})_2(\text{MA})_3\text{Pb}_4\text{I}_{13}$  with nominal “ $n = 4$ ,” but found that the sample is a mixture of multiple perovskite phases. As shown in Fig. 2a, the absorption peaks at  $\sim 572$ , 608, 645 and 750 nm can be assigned to pure phase  $(\text{BA})_2(\text{MA})_{n-1}\text{Pb}_n\text{I}_{3n+1}$  with  $n = 2, 3, 4$  and  $\infty$ , respectively [59]. Combined with the absorption and PL spectra (Fig. 2a, b), it can be inferred that the bottom is conducive to the formation of low  $n$  phase, and high- $n$  phase is easy to form at the top. For display and lasing applications with high color purity, it is necessary to accurately control 2D perovskites with specific  $n$  value, which can be obtained by growing single crystal. However, due to the fast nucleation rate of perovskites, the precise preparation of perovskite films with specific  $n$  value is still a worldwide scientific problem. Recently, Huang et al. introduced  $n$ -butylamine acetate to replace the traditional  $n$ -butylamine iodide to obtain phase-pure thin films. Figure 2c, d shows the absorption and PL spectra of the phase-pure RP perovskite films, which have obvious single peaks compared with the previous studies. The peak positions of the films are red shifted with the increase of  $n$  value [60, 61]. Chiu et al. [62] used tin-based and lead-based perovskites as research objects, added carboxylic acid in the anti-solvent, through the kinetic control of 2D perovskites nucleation process, inhibited the formation of thermodynamic favorable small  $n$  value and improved the selectivity for 2D perovskites with specific  $n$  value. It can be seen from Fig. 2e that the addition of hexanoic acid significantly suppress the formation of  $(\text{BA})_2\text{PbBr}_4$  ( $n = 1$ ). Interestingly, the control of hexanoic acid is not limited to the synthesis of  $n = 2$  phase-pure perovskites. The  $n = 3$  perovskite nanoplates can also be obtained by reducing the molar ratio of butylamine hydrobromide (Fig. 2f).



**Fig. 2** **a** UV–Vis absorption spectra of  $(\text{BA})_2(\text{MA})_3\text{Pb}_4\text{I}_{13}$  perovskite film. **b** Comparison of the emission spectra of the 2D perovskite film illuminated from the front and back sides of the film. Copyright 2018 American Chemical Society [59]. **c** Normalized UV–Visible absorption spectrum of the phase-pure films. **d** Normalized PL spectrum of the phase-pure films. Copyright 2020 Springer Nature [60]. Photoluminescence spectra (375 nm excitation) for the system using **e** BABr: MABr:  $\text{PbBr}_2 = 1.5: 0.5: 1$  and **f** BABr: MABr:  $\text{PbBr}_2 = 1.1: 0.5: 1$  molar ratio precursor. Copyright 2021 Wiley–VCH GmbH [62]

Compared with 3D perovskites, 2D perovskites not only have dimensional changes, but also have natural quantum well structures [63]. As shown in Fig. 1b,  $n$  represents the number of  $[\text{BX}_4]^{2-}$  octahedron layers, which can determine the well width and band gap. The larger the  $n$  value, the smaller the band gap. The  $[\text{BX}_4]^{2-}$  sheet can be regarded as a potential well, and the large organic cation acts as a potential barrier. And the barrier width is determined by the radius of the large organic cation. Through the self-assembly from

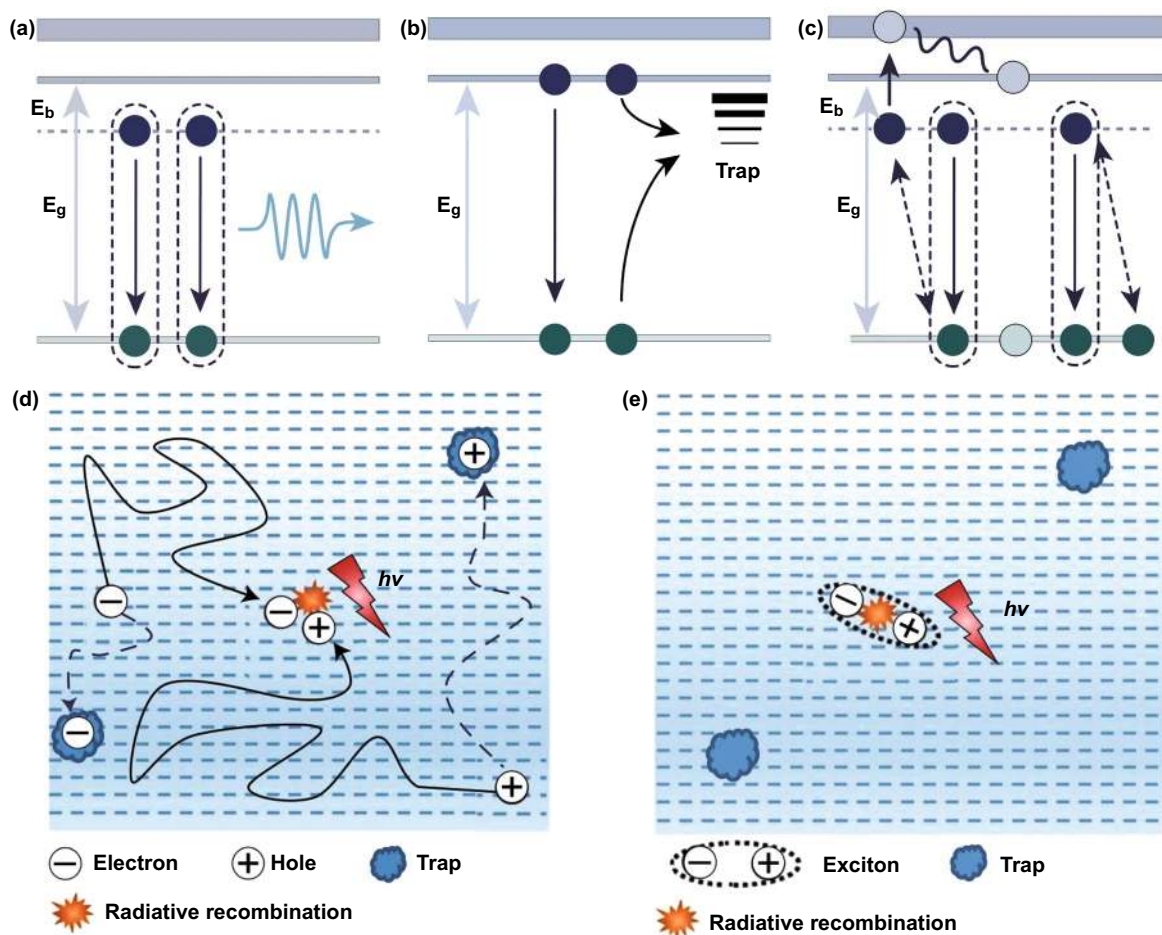
bottom to top, the organic–inorganic layers are arranged alternately to form multiple quantum well structures naturally. In addition, the  $E_b$  of 2D perovskites are larger than that of 3D perovskites due to the large difference of dielectric constants between organic and inorganic layers. Generally, the 2D layered perovskites contain many different components (marked by  $n$  value). The quantum wells have an ultra-fast energy transfer process; the transfer efficiency is close to 100% (sub nanoscale), which effectively inhibits

exciton quenching and makes the quantum well films exhibit high photoluminescence quantum efficiency (PLQY) under low excitation [64, 65]. Di et al. [44] achieved PeLED comparable to organic light-emitting diodes (OLEDs) and quantum dot light-emitting diodes (QD LEDs) by enhancing outcoupling with polymer additives, with EQE as high as 20.1% at 0.1–1 mA cm<sup>-2</sup>.

### 2.3 Charge-Carrier Recombination Kinetics

From the material point of view, the PLQY and photo-excited charge-carrier lifetime of perovskite materials are closely associated with the realization of efficient PeLED [30, 66, 67]. In Eq. 1,  $R_r$  and  $R_{nr}$  are radiative and non-radiative recombination rates, respectively. In perovskite, radiative recombination can be band-to-band

recombination or exciton recombination, while non-radiative processes are Shockley–Read–Hall (SRH) recombination and multiparticle interaction recombination (three body Auger recombination) (Fig. 3). The kinetics of carrier recombination in 3D perovskites can be summarized by Eq. 2.  $n$  is the charge-carrier density,  $t$  is the time,  $k_1$  is the trap-assisted monomolecular recombination rate constant (SRH),  $k_2$  is the bimolecular recombination rate constant (band-to-band recombination), and  $k_3$  is the three body Auger recombination rate constant; among them,  $k_1$  is usually affected by carrier confinement and defects, and  $k_2$  and  $k_3$  are intrinsic values. Carrier density determines which recombination is dominant. It is well known that free carriers are dominant in 3D perovskites because of their small  $E_b$ , which is close to room temperature thermal energy. This indicates that the excitons will dissociate into



**Fig. 3** **a** Exciton recombination. **b** Trap-assisted recombination. **c** Auger recombination. Copyright 2021 Springer Nature [72]. A schematic illustration of charge-carrier recombination **d** in 3D perovskites and **e** in 2D perovskites. Copyright 2020 Springer Nature [71]

free carriers at room temperature, so the radiative recombination in 3D perovskite is mainly controlled by the band-to-band recombination  $k_2$  [68]. As expressed in Eq. 2, the relationship between carrier recombination kinetics and carrier density is inseparable in 3D perovskites. Due to the slow band-to-band recombination rate (Fig. 3d), trap-assisted monomolecular recombination ( $k_1$ ) is dominant at low carrier density, and free carriers are easy to be trapped by defects. If the carrier density is high, the traps are full of free carriers and reach saturation states, which promotes bimolecular radiative recombination and improves PLQY.

$$\text{PLQY} = \frac{\sum R_r}{\sum R_r + \sum R_{nr}} \quad (1)$$

$$-\frac{dn}{dt} = k_1n + k_2n^2 + k_3n^3 \quad (2)$$

It is a pity that the charge-carrier density in typical 3D PeLED is usually less than  $10^{15} \text{ cm}^{-3}$ , which severely limits the rate of radiative recombination [48]. Reducing the size or dimension (such as 2D, 1D) of perovskite crystals can effectively increase the charge-carrier confinement [69, 70]. From the above point of view, 2D perovskites are an ideal candidate for PeLED. Unlike 3D perovskites, 2D perovskites have exciton binding energies as high as several hundred milli-electron volts. As shown in Fig. 3e, the excitons are stable and difficult to separate into free carriers at room temperature, which directly leads to the rapid radiative monomolecular recombination rates [41], and hence, the relationship between the carrier recombination dynamics and the carrier density changes correspondingly. Equation 2 is not suitable for 2D perovskites, and this relationship is shown in equation [71]. Where  $k_{\text{trap}}$  is non-radiative monomolecular recombination rate constant,  $k$  is radiative monomolecular recombination rate constant and  $k_2$  is the rate constant of Auger recombination. From Eq. 3, it can be seen that the influence of carrier density on carrier recombination kinetics is reduced. In 2D perovskite, excitonic recombination not only competes with non-radiative monomolecular recombination, but also competes with Auger recombination.

$$-\frac{dn}{dt} = (k_{\text{trap}} + k)n + k_2n^2 \quad (3)$$

## 2.4 Advantages of 2D Perovskite as Light-Emitting Layer

It is well known that high PLQY is the key factor to realize efficient PeLEDs. The  $E_b$  of 2D perovskites is large, which promotes the enhancement of radiative recombination rate. PLQY is also strongly dependent on defect density. The decrease of defect density can reduce the possibility of non-radiative recombination. In essence, the problem of low luminescence efficiency of materials is solved. Furthermore, the high-quality film morphology and balanced bipolar charge injection are the key factors to determine the EQE of PeLEDs, because the compact films can effectively reduce the leakage current. It was found that large organic cations are favorable for the formation of uniform pinhole-free films in 2D perovskite [73].

### 2.4.1 Excitonic Characteristics and Ultra-Fast Energy Transfer

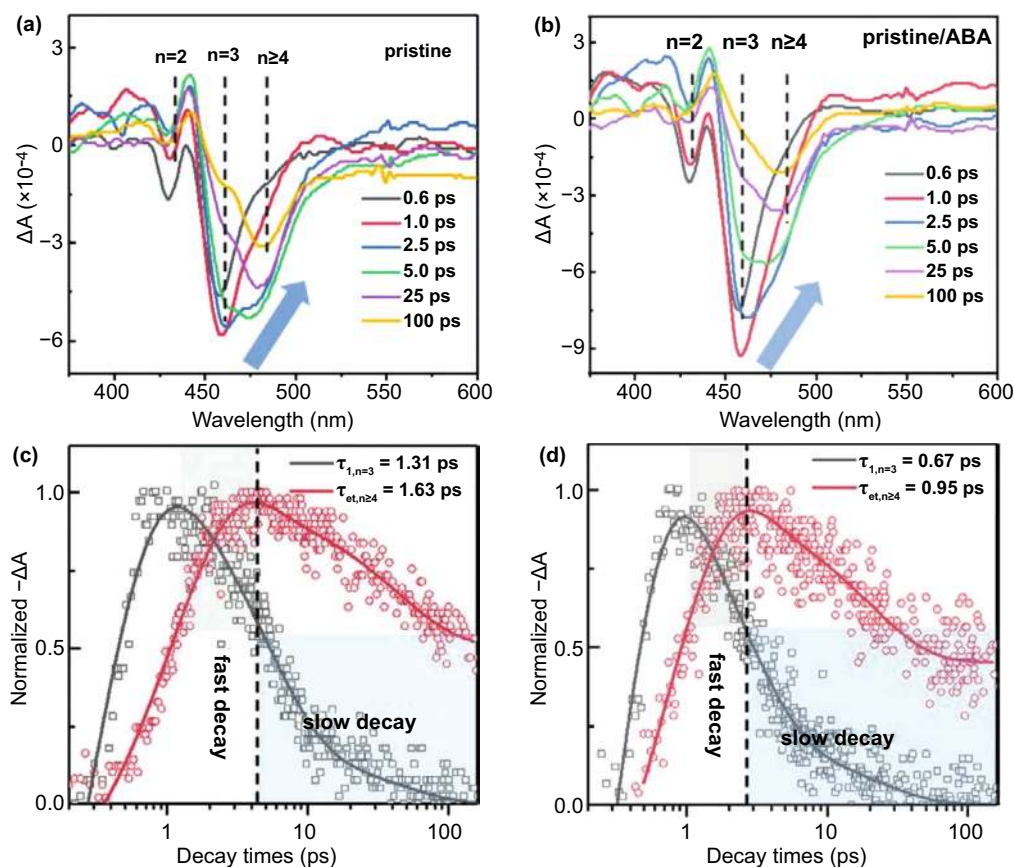
3D perovskites usually have a small  $E_b$ , which is unfavorable for LEDs [74]. Compared with 3D perovskites, 2D perovskites are affected by quantum confinement and dielectric confinement [75]. The effect of quantum confinement origin the close thickness of the  $[\text{BX}_6]^{4-}$  octahedral layers to the Bohr radius. The dielectric constant offset between organic cations and  $[\text{BX}_6]^{4-}$  octahedral layers results in the dielectric confinement effect. These effects are beneficial to the formation of bound excitons. Besides, the natural quantum well structure has ultra-fast energy transfer, so the carrier density increases and the shallow defects which affect the luminescence efficiency are filled. In 2D perovskites, the trap-assisted monomolecular recombination lost its competitiveness, and the first-order excitonic radiative recombination is dominant, and PLQY is improved [31]. Similar to the host-guest systems of OLEDs, energy transfer can occur among different samples with  $n$  values. The cascade energy transfer from the wide bandgap (small  $n$  value) to the narrow bandgap (large  $n$  value) can effectively avoid the concentration quenching and dramatically improve the radiative recombination rate in the maximum  $n$  value [42, 76]. Unfortunately, the quasi-2D perovskites are a mixture of many phases (especially a large number of small  $n$  phases),

resulting in inefficient energy transfer. Choy et al. introduced a bifunctional organic ligand (amino and carboxyl group) to weaken the van der Waals gap, which can contribute to the efficient energy transfer of perovskite films. As shown in the ultra-fast transient spectroscopy (TA) spectra (Fig. 4a, b), three distinctive ground-state bleach peaks corresponding to  $n=2$ , 3 and  $\geq 4$  are observed at 428, 453 and 481 nm, respectively. With increasing decay time, the ground-state bleach peak value of the small  $n$  phase gradually decreases, and that of the large  $n$  phase ( $n \geq 4$ ) gradually increases, indicating that carriers transfer from small  $n$  phase to large  $n$  phase. Further,  $n=3$  phase and  $n \geq 4$  phase are selected as the research objects, and the kinetic multi-exponential function fitting is carried out. Both  $n=3$  ( $\tau_{1,n=3} = 0.67$  ps) and  $n \geq 4$  ( $\tau_{\text{et},n \geq 4} = 0.95$  ps) in the pristine/ABA perovskites show smaller values, which are about half of the pristine perovskites ( $\tau_{1,n=3} = 1.31$  ps;  $\tau_{\text{et},n \geq 4} = 1.63$  ps), implying that more

efficient energy transfer is achieved (Fig. 4c, d). Moreover, the carrier transfer is completed in picoseconds [77]. Lee et al. [43] also observed a similar result, and the enhancement of energy transfer is favorable to reduce the probability of non-radiative recombination, thus improving the device performance. Although the mechanism of photogenerated electron and hole transfer is still controversial, the rapid carrier transfer process can compete with trap-assisted monomolecular non-radiative recombination, which makes the quasi-2D perovskite structure beneficial to enhance PLQY [78, 79].

#### 2.4.2 Dense Film Morphology

The morphology of perovskite films is a key factor to determine the performance of PeLEDs. Generally, 3D perovskite thin films have rough surface and are prone to a large



**Fig. 4** TA spectroscopy of **a** the pristine and **b** pristine/ABA perovskite films. TA kinetics probed at selected wavelengths (453 and 481 nm) for **c** pristine and **d** pristine/ABA perovskite films. Copyright 2020 Wiley-Blackwell [77]

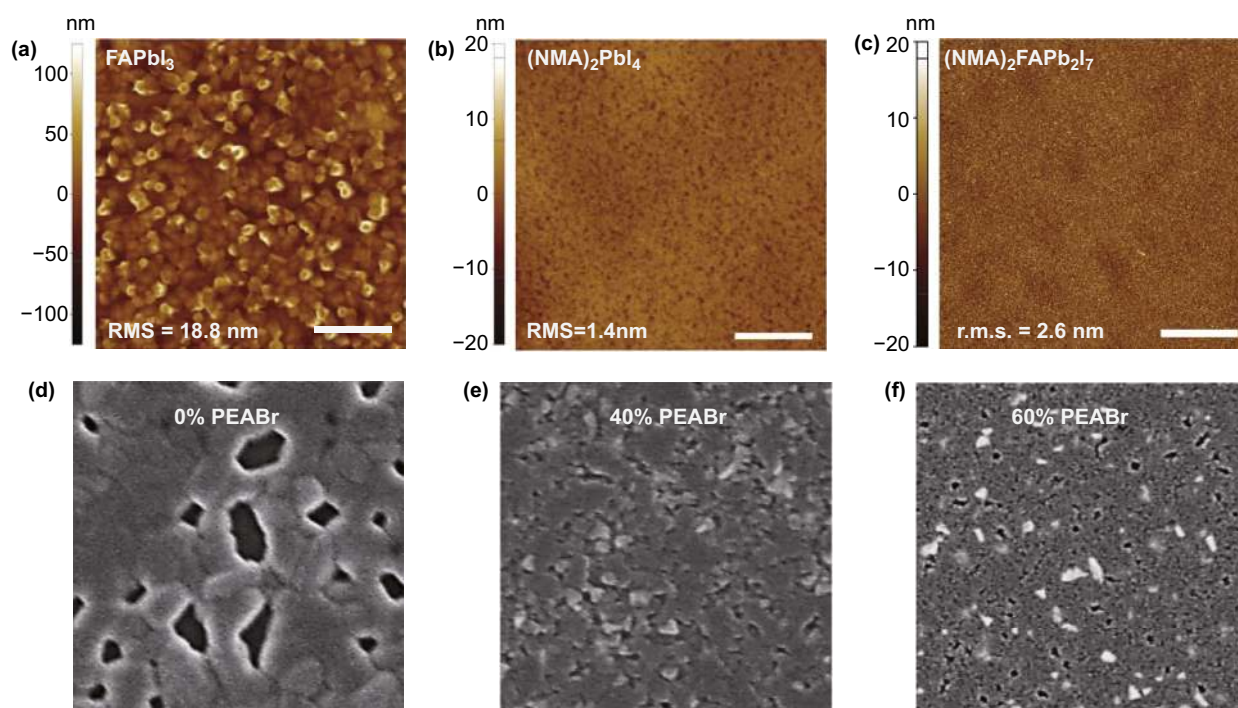


number of pinholes, leading to the increase of leakage current and obvious thermal effect, which will be resulting in the decrease of device efficiency and the shortening of device life [80, 81]. The results show that 2D perovskites have better film morphology than 3D perovskites. Organic cations can improve the morphology of 3D perovskite films and promote the formation of dense pinhole-free films [78, 82, 83]. For example, the root-mean-square roughness of 3D FAPbI<sub>3</sub> perovskite film is 18.8 nm. Surprisingly, the root-mean-square roughness of 2D (NMA)<sub>2</sub>PbI<sub>4</sub> ( $n=1$ ) and (NMA)<sub>2</sub>FAPb<sub>2</sub>I<sub>7</sub> ( $n=2$ ) films is 1.4 and 2.6 nm, respectively (Fig. 5a–c) [42]. In addition, Cao et al. improved the surface coverage of CsPbCl<sub>0.9</sub>Br<sub>2.1</sub> film by introducing PEABr, with only a few small pinholes (Fig. 5d–f). More importantly, if PEABr is replaced by other amines, a similar phenomenon will be observed [84].

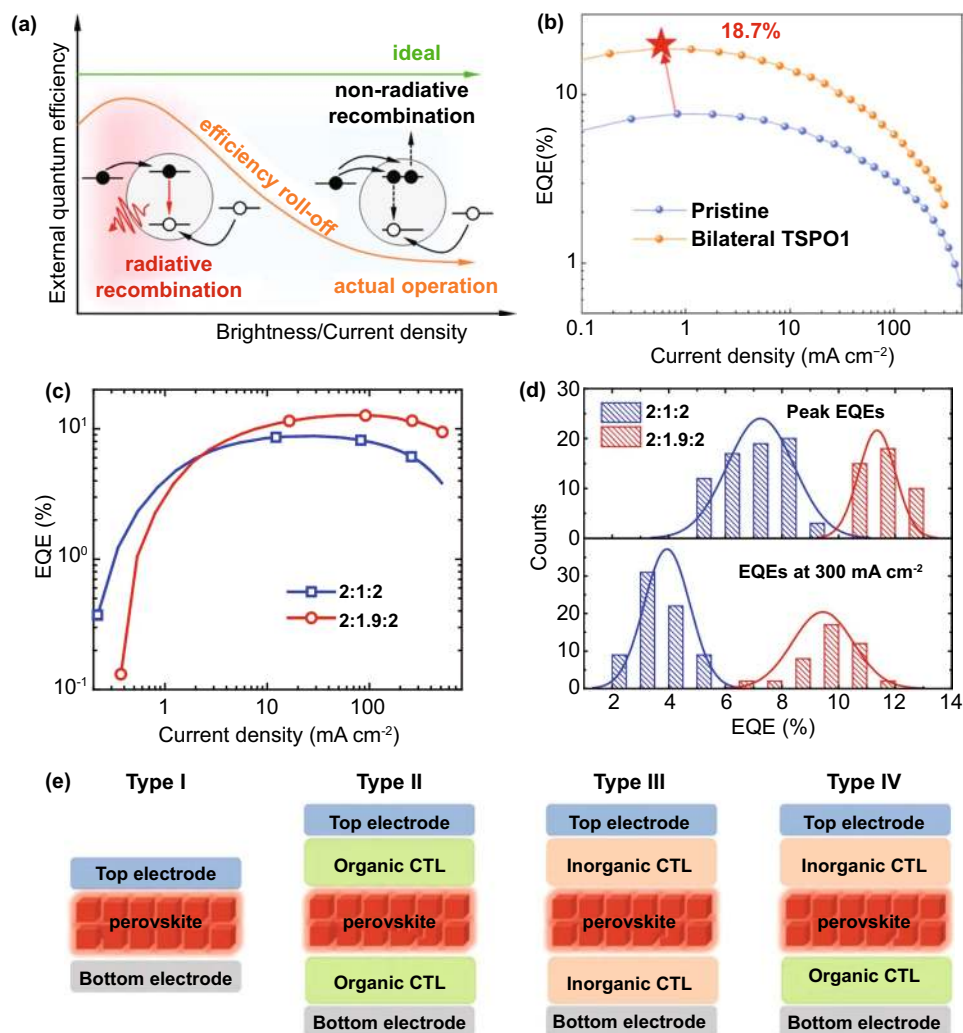
#### 2.4.3 Lower Efficiency Roll-Off

At present, the EQE of classical perovskite material CsPbX<sub>3</sub> ( $X=Cl^-$ ,  $Br^-$ ,  $I^-$ ) has exceeded 20% [85]. However, as shown in Fig. 6a, with increasing brightness and

current density, the EQE of devices tends to decrease, which is called efficiency roll-off. In particular, due to the exciton effect, the efficiency rolls off of perovskite quantum dots are very serious at high current density [86]. Zeng et al. [87] used organic molecules to passivate the top and bottom of perovskite quantum dot film, which improved the stability of PeLEDs and effectively suppressed the non-radiative recombination. The EQE was as high as 18.7% at low current density. Unfortunately, at a high current density of 100 mA cm<sup>-2</sup>, the EQE value is only 32% of the maximum value (Fig. 6b). Sargent et al. [88] proposed to construct a bipolar shell composed of inner anion shell on the surface of perovskite quantum dots. More than 90% of PLQY blue quantum dot films were obtained. Surprisingly, the maximum EQE value is 12.3%, but there is also a large efficiency roll-off value. For most devices, the decrease of EQE at high current density is due to the combination of charge injection imbalance, Auger-induced luminescence quenching and Joule heating [89, 90]. Perovskite quantum dots LEDs have severe efficiency roll-off because of Auger recombination at low current density. However, in quasi-2D perovskite,



**Fig. 5** AFM height images of **a** FAPbI<sub>3</sub> **b** (NMA)<sub>2</sub>PbI<sub>4</sub> and **c** (NMA)<sub>2</sub>FAPb<sub>2</sub>I<sub>7</sub> films (scale bar 5 μm). Copyright 2016 Springer Nature [42]. SEM images of perovskite films with **d** 0% PEABr **e** 40% PEABr and **f** 60% PEABr. Copyright 2019 Springer Nature [84]



**Fig. 6** **a** Efficiency roll-off under ideal and actual PeLEDs operating conditions. Copyright 2020 American Chemical Society [100]. **b** EQE of original and bilateral-passivated device. Copyright 2020 Springer Nature [87]. **c** EQE versus current density. **d** Histograms of peak EQEs and EQEs at  $300 \text{ mA cm}^{-2}$ . Copyright 2018 Springer Nature [91]. **e** Schematic diagrams of the four device structures of PeLEDs. Copyright 2019 Wiley–VCH Verlag Copyright 2019 Wiley–VCH Verlag [85]

Auger recombination can be suppressed by reducing the local carrier density in the quantum well. Huang et al. [91] changed the width of perovskite quantum wells by controlling the proportion of organic cations without reducing the luminescence performance. The results show that increasing the well width can significantly suppress the luminescence quenching effect. As shown in Fig. 6c, the maximum EQE values of 2:1:2 and 2:1.9:2 devices are 8.7% and 12.7%, respectively. Furthermore, the efficiency roll-off of 2:1.9:2 device is effectively suppressed; even at  $500 \text{ mA cm}^{-2}$ , it can still maintain 10% of the peak

value. In addition, compared with 2:1.9:2 device (5.7%), the relative standard deviation of 2:1:2 device is larger (16.3%). Under the same current density ( $300 \text{ mA cm}^{-2}$ ), the average EQE value of 2:1.9:2 device is more than twice that of 2:1:2 device (Fig. 6d). Although adjusting the well width can effectively reduce the efficiency roll-off, compared with the 3D PeLEDs, quasi-2D PeLEDs also suffer from serious efficiency roll-off. The strategies of reducing the roll-off effect of quasi-2D PeLEDs will be discussed in details in the next section.

### 3 Strategies for Boosting the Performance of PeLEDs

#### 3.1 Suppression of Efficiency Roll-Off

As we all know, quasi-2D perovskite materials are expected to be candidates for the next-generation display applications [58, 92]. Unfortunately, the quasi-2D perovskite materials suffer from serious efficiency roll-off, which is mainly caused by the charge injection imbalance, Auger recombination and Joule heating [93].

##### 3.1.1 Balance of Charge Injection

High PLQY is the key factor to realize efficient and stable 2D PeLEDs. Other key elements include effective charge injection, defect passivation and ion migration suppression. Currently, for PeLEDs devices, there is no unified name for the device structures, which are usually divided into formal and inverted device structures. Rogach et al. adjusted the classification of PeLEDs device structures on the basis of Cd-based QD LEDs. As shown in Fig. 6e, type I has no charge transport layer, charge transport layers of type II are all organic polymers/small molecules, charge transport layers of type III are all inorganic, and organic and inorganic molecules of type IV are used as charge transport layers [85]. For 2D PeLEDs, the device structures of type I and III are rarely reported, while type II and IV are mostly studied.

The charge injection imbalance is related to the injection barrier [94], carrier mobilities [95] and defect density [96]. The relationship between barrier height and electric current can be seen from Eqs. 4 and 5

$$J \propto E^2 \exp\left(\frac{-b}{E}\right) \tag{4}$$

$$b = \frac{8\pi\sqrt{2m^*\varphi^2}}{3qh} \tag{5}$$

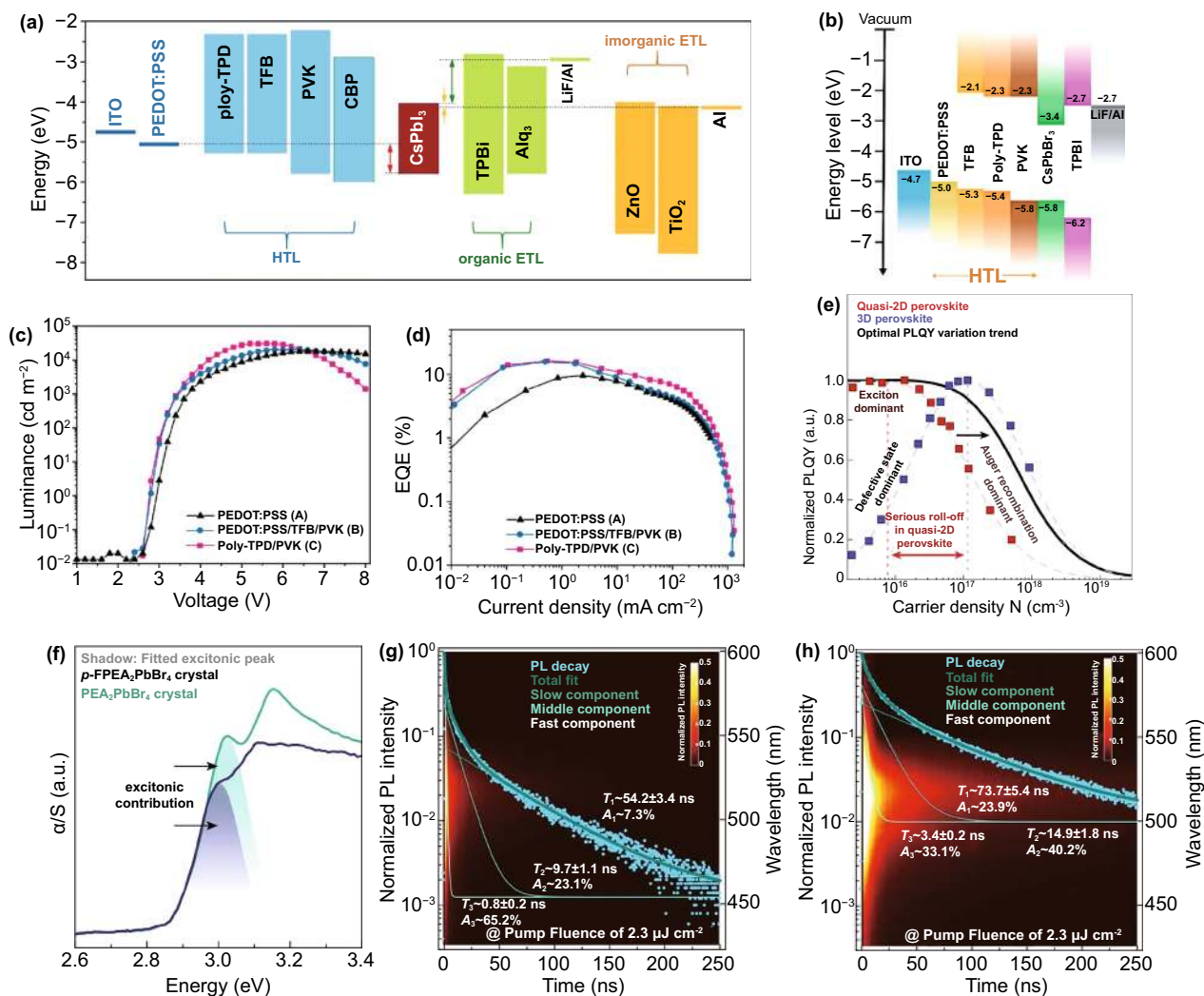
where  $J$  is the current density,  $E$  is the electric field,  $\varphi$  is the barrier height,  $m^*$  is the carrier effective mass,  $q$  is the element charge, and  $h$  is the Planck constant [97]. The work function of the cathode is different from that of the conduction band bottom of the electron transport layer (ETL). Similarly, the difference also exists in the work function of the anode and the top of the valence band of the hole transport layer (HTL), resulting in potential barrier. To overcome the

barrier, the charge carrier must have enough energy. The relationship between barrier height and luminous efficiency can be seen in Eq. 6.

$$\text{Efficiency} \propto \exp\left(\frac{-r\varphi^3}{V}\right) \tag{6}$$

where  $V$  is applied bias and  $r$  is constant. The turn-on voltage and luminous efficiency of the device are affected by the barrier heights of the interfaces and the semiconductor energy levels of each layer. The turn-on voltage is closely associated with the flat band conditions determined by the work functions of cathode and anode. For 2D PeLEDs, it can be seen from Eq. 6 that the charge injection with a small energy barrier is a necessary condition to obtain low operating voltage and high luminous efficiency. Also, the stability of 2D PeLED is also going hand in hand with effective carrier injection. Invalid carrier injection will lead to charge imbalance and space charge accumulation in perovskite emitting layer. Thus, it is very important to match the energy levels at the interfaces [98]. For most PeLEDs, high electron injection efficiency and low hole injection efficiency lead to the imbalance of charge injection, which seriously affects the performance of PeLEDs [99, 100]. As shown in Fig. 7a, taking CsPbI<sub>3</sub> as an example, there is a high barrier between HTL and emitting layer, and holes need to overcome it to successfully transport to emitting layer (red arrow). However, ETL is different from HTL. For inorganic ETL, only a very small barrier needs to be overcome to reach the perovskite layer (yellow arrow). Furthermore, for organic ETL, electrons can be easily transported to the emitting layer due to the additional driving force (green arrow) [100]. At a low current density, more radiative recombination can be maintained with less carrier injection. At a high current density, the number of carriers injected increases, and the electron hole pairs are easily quenched between the HTL and the emitting layer due to the mismatch of energy levels [101]. Lin et al. established “energy ladder” in HTL to solve the problem of charge injection imbalance (Fig. 7b). It can be seen from Fig. 7c that the maximum luminance of multilayer HTL devices (PEDOT: PSS/TFB/PVK, poly-TPD/PVK) is 20342 and 31,012 cd m<sup>-2</sup>, respectively, while the maximum luminance of single-layer HTL device (PEDOT: PSS) is only 18,154 cd m<sup>-2</sup>. The establishment of “energy ladder” is helpful to improve the efficiency of hole injection and reduce the turn-on voltage. It is gratifying that the EQEs of multilayer HTL devices have also been greatly improved (Fig. 7d), and the efficiency roll-off of poly-TPD/PVK is suppressed at the current density of 0.01–1000 mA cm<sup>-2</sup> [102].

Although balanced charge injection can suppress the efficiency roll-off, there is still a serious efficiency roll-off at a



**Fig. 7** **a** Schematic diagram showing energy levels of typical electrodes, charge transport materials and CsPbI<sub>3</sub>. Copyright 2020 American Chemical Society [100]. **b** Energy level diagrams of quasi-2D PeLEDs and different HTLs. **c** L-V and **d** EQE-J of PEDOT: PSS, PEDOT: PSS/TFB/PVK, poly-TPD/PVK. Copyright 2020 American Chemical Society [102]. **e** Experimental PLQYs of quasi-2D perovskite and 3D perovskite films as a function of carrier density. **f** Absorption spectra of PEA<sub>2</sub>PbBr<sub>4</sub> and p-FPEA<sub>2</sub>PbBr<sub>4</sub> single crystals. Time- and wavelength-dependent photoluminescence mapping under a pump fluence of 2.3 μJ cm<sup>-2</sup> for **g** PEA and **h** p-FPEA films. Copyright 2021 Springer Nature [72]

high current density, which may be due to the existence of long organic chains, resulting in poor charge transport, or the increase of Auger recombination rate due to the quantum well structures.

### 3.1.2 Reducing of Auger Recombination

Auger recombination is affected by carrier density, as shown in Eq. 7, where  $g_{\text{eeh}}$  is the Coulomb enhancement factor, and the value is associated with  $E_{\text{b}}$ .  $k_{\text{Auger}}^0$  is the band-to-band Auger recombination rate (non-interact

particles),  $C_n$  is the Auger coefficient, and  $n$  and  $P$  are the electron density and hole density, respectively.

$$k_{\text{Auger}} = g_{\text{eeh}} k_{\text{Auger}}^0 = g_{\text{eeh}} C_n n^2 p \quad (7)$$

As shown in Fig. 7e, the black curve is an ideal evolution trend of PLQY. The curve trend of the quasi-2D perovskites is highly similar to that of the black curve. Even at a low current density, the quasi-2D perovskites can obtain high PLQY. However, compared with 3D perovskites, Auger recombination of quasi-2D perovskites is very severe. That is because the carrier density of

3D perovskites is lower than that of quasi-2D perovskites [41, 103]. From Eq. 7, it can be concluded that the Auger recombination rate is positively related to the third power of carrier density, so the Auger recombination rate of quasi-2D perovskites increases. The other reason is due to the enhanced electron hole interaction, which leads to the non-uniform distribution of carriers [104, 105]. Yuan et al. increased the dielectric constant of organic cations to weaken the “dielectric confinement effect,” which not only significantly reduced  $E_b$ , but also did not change the energy transfer efficiency. Using highly polarized  $p$ -FPEA<sup>+</sup> to replace the A site in the classical quasi-2D perovskite material PEA<sub>2</sub>MA<sub>n-1</sub>Pb<sub>n</sub>Br<sub>3n+1</sub>, the molecular dipole moment is increased (simulated by density function theory), which is conducive to charge separation. Strong evidence for the decrease of  $E_b$  is found in the optical absorption spectra. As shown in Fig. 7f, PEA<sub>2</sub>PbBr<sub>4</sub> has an obvious excitonic peak at about 3.08 eV, while only a small kink (3.04 eV) is observed in  $p$ -FPEA<sub>2</sub>PbBr<sub>4</sub>. Moreover, the  $E_b$  values are estimated quantitatively by temperature-dependent photoluminescence measurements. And the  $E_b$  values of PEA<sub>2</sub>PbBr<sub>4</sub> and  $p$ -FPEA<sub>2</sub>PbBr<sub>4</sub> are 347 and 195 meV, respectively. To further strengthen this conclusion, multi-exponential fitting is used to analyze the carrier dynamics at a high current density (up to  $\sim 1 \times 10^{17} \text{ cm}^{-3}$ ). The fastest decay is associated with Auger recombination. The fast decay times of Auger recombination for PEA and  $p$ -FPE samples are 0.8 and 3.4 ns, respectively (Fig. 7g, h). Thus, Auger recombination rate decreased significantly. Unfortunately, while Auger recombination decreased, PLQY also decreased significantly. On the basis of previous study, molecular passivation (another strategy) was used to reduce trap-assistant recombination. Finally, the device showed a record luminance ( $82,480 \text{ cd m}^{-2}$ ) [72].

### 3.2 Passivation of Surface Defects

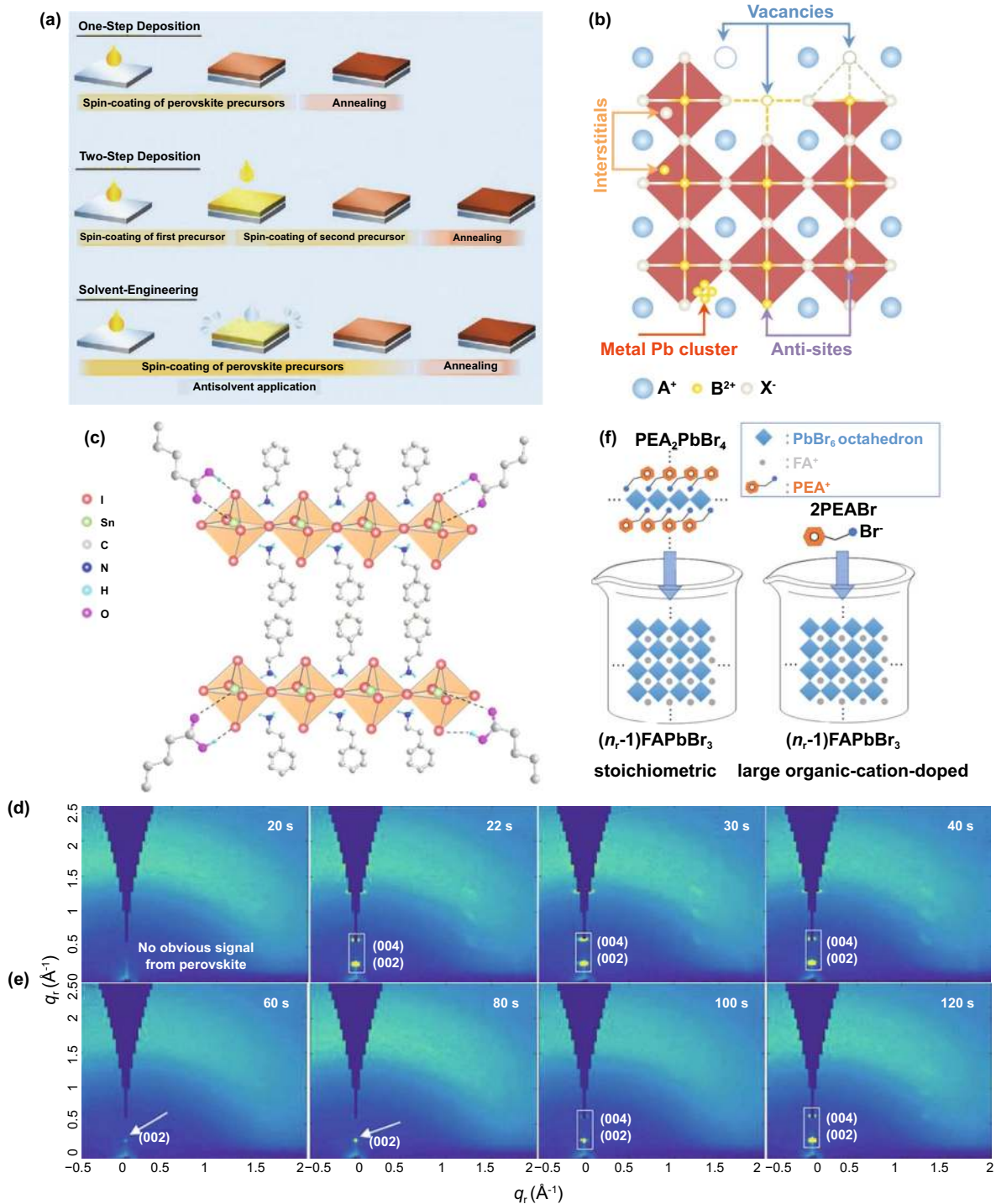
At present, a large number of research reports regard solution processing as the deposition method of PeLEDs [106, 107]. Solution processing has significant advantages, such as high cost-effectiveness, simple process and no need for a complex vacuum system [108, 109]. It has broad application prospects in PeLEDs. General solution-processing methods include one-step, two-step and solvent engineering methods

(Fig. 8a) [107]. Solvent engineering is the most widely used method so far, which is based on the one-step method, adding anti-solvent to promote the crystallization of perovskite films [110]. However, solution-processing perovskite materials suffer from severe non-radiative recombination (caused by traps), which seriously limits the application and development of PeLEDs [111, 112]. Trap states are generally considered to be related to ionic defects, such as vacancies, anti-site occupations and interstitials (Fig. 8b) [71]. Using passivation agents to passivate defects is a very effective method, which has been determined to reduce the defect density and non-radiative recombination of perovskites. Usually, the passivation agents are added at the beginning of the reaction or in the post-treatment. Common passivation agents include Lewis acid/base and organic halide salts [113]. For example, Sargent et al. produced high-efficiency, lead-free PeLED by adding valeric acid (VA). The EQE is 5%, and the half-life is exceeding 15 h. That is so due to strong forces, of hydrogen bonds (O=C–OH...I<sup>-</sup>) and coordination bond (C=O...Sn<sup>2+</sup>) between VA and PEA<sub>2</sub>SnI<sub>4</sub> thin films (Fig. 8c). The existence of the interaction forces inhibits the rapid nucleation and slows down the crystallization rate, thus forming a uniform pinhole-free morphology (Fig. 8d, e). And VA can also be used to inhibit the oxidation of tin in the process of film formation [114]. Moreover, Adachi et al. systematically compared the effects of controlling stoichiometry and adding organic ammonium salts on the surface defects and domain distribution of the films with quasi-2D perovskites (Fig. 8f). The results show that PEA<sup>+</sup> cations in the stoichiometric control method mainly play the role of passivation. In contrast, adding a large amount of PEABr in 3D perovskite precursor can not only passivate the surface defects but also inhibit the appearance of small  $n$  values, which is helpful to the formation of quasi-2D perovskite domains. It is well known that low-order domains damage the performance of PeLEDs. Therefore, perovskite films with organic ammonium salts have higher defect passivation efficiency and higher EQE [115].

### 3.3 Critical Role of Organic Cations for PeLEDs

#### 3.3.1 Reasonable Selection of Organic Cations

It is universally acknowledged that 2D perovskites can still show better stability than 3D perovskites when exposed to moisture, which is due to the hydrophobicity of organic



**Fig. 8** **a** Schematic diagram of perovskites deposition by solution processing. Copyright 2020 Wiley–VCH Verlag [107]. **b** Defects of perovskites include vacancies, anti-sites, interstitials and metal clusters. Copyright 2020 Springer Nature [71]. **c** Diagram of hydrogen bonding and coordination bonding interactions between VA and PEA<sub>2</sub>SnI<sub>4</sub> crystals. In situ GIWAXS measurements of spin-coated PEA<sub>2</sub>SnI<sub>4</sub> **d** without and **e** with VA at different times. Copyright 2020 American Association for the Advancement of Science [114]. **f** Illustration of perovskite precursor solutions prepared by controlling stoichiometry and adding organic ammonium salts. Copyright 2020 Wiley–VCH Verlag [115]

cations. And there is a strong interaction between the organic cations and the capped organic molecules. Moreover, the chain lengths and  $\pi - \pi$  stacking of organic cations affect the  $n$  distribution of 2D perovskites [116–118]. A variety of organic cations, such as butylammonium (BA) [119], phenylethylammonium (PEA) [120], 1-naphthylmethylammonium (NMA) [120] and benzimidazolium (BIZ) [121], have been studied (Table 1). Unfortunately, most of the research reports focus on a specific ion. There are some questions about which organic cation should be selected, and the device design is not reasonable.

Jin et al. selected two different organic cations, namely PBA and BA. Through comparison, it was found that different organic amine cations would affect the thicknesses of perovskite quantum wells, efficiency of energy transfer and recombination kinetics, resulting in great differences in the performance of PeLEDs [122]. Similarly, Nie et al. deeply discussed the influence of organic cations with benzyl ring (PEA) or alkyl chain (BA) as spacer on PeLEDs. It is found that the carrier lifetime of PEA-based film is 5 times that of BA-based film (Fig. 9a), which greatly improves the probability of radiative recombination. It is worth noting that the luminance of benzyl ring is 70 times that of alkyl chain, and it has superior output luminance efficiency (about 25 cd  $A^{-1}$ ) and EQE (more than 9%). The results show that such a large difference is closely related to the steric hindrance of organic cations. Compared with alkyl chain, the volume of benzyl ring is larger, which will affect the crystalline packing of inorganic layers. Because the alkyl chain is more flexible, the band structure of perovskite will not be affected. The time-resolved X-ray absorption spectra show that the hole localization signal of benzyl ring film is near the Br  $p$ -orbital, which increases the carrier lifetime and enhances the radiative recombination efficiency (Fig. 9b–d). Therefore, the PeLEDs of benzyl ring show excellent electroluminescent properties. However, these were not observed in the alkyl chain film [123]. In addition, Wang et al. selected the organic cation BIZ without alkyl branches by comparing the  $d$ -spacing of various organic cations (Fig. 9e). Because the smaller the  $d$ -spacing, the shorter the barrier width, which can increase the carrier mobility. Figure 9f shows that BIZ has excellent electron mobility and hole mobility [124]. Using the same method, Pullerits et al. [125] selected iso-BA with smaller  $d$ -spacing, which significantly increased the transfer rate and reduced the possibility of charge accumulation. Choosing different organic cations will

change the intrinsic electronic properties of semiconductors [126], which is helpful to design highly efficient and stable PeLEDs. So far, the choice of spacer cations is not limited to a single organic ion. Various mixed organic cations as spacers have been reported in many excellent works. Choy et al. introduced the bifunctional organic spacer 4-(2-Aminoethyl) benzoic acid (ABA) into  $PEA_xPA_{2-x}(CsPbBr_3)_{n-1}PbBr_4$ . Due to the addition of ABA, the interaction between the layers of perovskite was enhanced, and Pb was suppressed to reduce the trapped states and promote the reduction of non-radiative recombination loss. The blue 2D PeLEDs with good performance (EQE = 8.21%) and high stability ( $T_{50}$  = 81.3 min) were obtained [77]. From the perspective of theoretical calculation, taking  $n = 2$  as an example, the performance of mixed organic cation LEDs is better than that of single spacer cation LEDs, which is attributed to lower formation energy, lower strain and lower electron–phonon coupling [21].

In a word, the chain length, size and properties of organic cations may affect the performance of the device. Compared with alkyl chain, organic cations with large volumes are selected, such as traditional  $PEA^+$  and  $PBA^+$ . The higher the molecular packing density in the organic layer is, the higher the rigidity of the crystal will be. Sargent et al. showed that 2D perovskite single crystals with high PLQY and good quality can be obtained by controlling the crystal rigidity [74]. In addition, the selection of organic cations with small spacing also helps to increase PLQY, which is due to the decrease of the barrier width of charge transport and the increase of carrier mobility.

### 3.3.2 Adjusting Width of Quantum Well

As we known, effective energy transfer plays a decisive role in the photoluminescence efficiency of 2D perovskites. Reasonable distribution of quantum well width can reduce unnecessary energy loss and facilitate carrier transport. To achieve high-performance PeLEDs, it is necessary to study the influence of quantum well width distribution on devices. Zhong et al. controlled the  $n$  values of perovskite films by adjusting the ratio of DPPABr to PEABr. Figure 10a shows that the larger the DPPABr/PEABr ratio is, the larger the  $n$  domains are. Interestingly, there are multiple emissions when DPPABr content is the highest. DPPABr promotes the formation of large  $n$  domains, while

**Table 1** Various large organic cations in PeLEDs








| Cation  | Emitter material   | EL (nm)  | EQE <sub>max</sub> (%)                                  | L <sub>max</sub> (cd m <sup>-2</sup> )   | Year   | Refs   |
|---|--|--|---|--|--|--|
|    | PA <sub>2</sub> CsPb <sub>2</sub> I <sub>7</sub> ; CsPb(Br,Cl) <sub>3</sub>  | 693  | /   | /  | 2018   | [127]  |
|    | PA <sub>2</sub> (CsPbBr <sub>3</sub> ) <sub>n-1</sub> PbBr <sub>4</sub><br>PA <sub>2</sub> (CsPbBr <sub>3</sub> ) <sub>n-1</sub> PbBr <sub>4</sub><br>BA <sub>2</sub> (CsPbBr <sub>3</sub> ) <sub>n-1</sub> PbBr <sub>4</sub> -PEO   | 492<br>~505<br>514                                 | 1.45<br>3.6<br>8.42                                     | 5737<br>7320<br>33,533   | 2019<br>2018<br>2018   | [128]<br>[129]<br>[130]  |
|    | BA <sub>2</sub> Cs <sub>n-1</sub> Pb <sub>n</sub> (Br/Y) <sub>3n+1</sub><br>BA <sub>2</sub> FA <sub>2</sub> Pb <sub>3</sub> Br <sub>10</sub> (n = 3)<br>n-BABr-MApPbBr <sub>3</sub><br>BA <sub>2</sub> Cs <sub>n-1</sub> Pb <sub>n</sub> Br <sub>3n+1</sub><br>(BA) <sub>2</sub> Cs <sub>n-1</sub> Pb <sub>n</sub> Br <sub>3n+1</sub><br>BA <sub>2</sub> Cs <sub>4</sub> Pb <sub>5</sub> Br <sub>16</sub><br>BA <sub>2</sub> MA <sub>n-1</sub> Pb <sub>n</sub> Br <sub>3n+1</sub><br>(C <sub>8</sub> H <sub>17</sub> NH <sub>3</sub> ) <sub>2</sub> (CH(NH <sub>2</sub> ) <sub>2</sub> ) <sub>m-1</sub> Pb <sub>m</sub> Br <sub>3m+1</sub> | 506<br>543<br>/<br>512<br>/<br>512<br>526.9<br>540 | 10.1<br>14.6<br>17.5<br>20.5<br>8.44<br>16.35<br>/<br>5 | 3810<br>24,100<br>48,668<br>13,400<br>3610<br>6785<br>~103<br>/<br>34,480<br>350 | 2018<br>2018<br>2019<br>2021<br>2020<br>2020<br>2020<br>2018 | [131]<br>[132]<br>[133]<br>[134]<br>[119]<br>[135]<br>[123]<br>[136] |
|    | (OA) <sub>2</sub> (FA) <sub>n-1</sub> Pb <sub>n</sub> Br <sub>3n+1</sub><br>(OAm) <sub>2</sub> SnBr <sub>4</sub>   | 528–532<br>625                                     | 13.4<br>0.1   | /  | 2018<br>2019   | [137]<br>[138]   |
|   | 100% PMA + CsPbBr <sub>3</sub>   | /  | 0.69  | 300  | 2020   | [139]  |
|  | (PEA) <sub>2</sub> PbCl <sub>2</sub> Br <sub>2</sub>   | 475  | /   | 70   | 2018   | [140]  |
|  |  |  |   |  |  |  |



Table 1 (continued)

| Cation | Emitter material  | EL (nm) | EQE <sub>max</sub> (%) | L <sub>max</sub> (cd m <sup>-2</sup> ) | Year | Refs  |
|--------|---|---------|------------------------|--|------|-------|
|        | 2D PEABr-CspBBr <sub>3</sub>  | 513     | 16.2                   | 31,012                                 | 2020 | [102] |
|        | PEA <sub>2</sub> SmI <sub>4</sub>   | 629     | 0.16                   | 58                                     | 2020 | [30]  |
|        | 60%EA: PEA <sub>2</sub> (CsPbBr <sub>3</sub> ) <sub>2</sub> PbBr <sub>4</sub>                             | 488     | 12.1                   | 2191                                   | 2020 | [141] |
|        | 40%EA: PEA <sub>2</sub> (CsPbBr <sub>3</sub> ) <sub>2</sub> PbBr <sub>4</sub>                             | 495     | 13.3                   | 2790                                   | 2020 | [141] |
|        | 80%EA: PEA <sub>2</sub> (CsPbBr <sub>3</sub> ) <sub>2</sub> PbBr <sub>4</sub>                             | 480     | 4.91                   | 83                                     | 2020 | [141] |
|        | (PEA) <sub>2</sub> (FA) <sub>n-1</sub> Pb <sub>n</sub> Br <sub>3n+1</sub>                                 | 532     | 14.36                  | 9120                                   | 2018 | [142] |
|        | PEA <sub>2</sub> (Rb <sub>x</sub> Cs <sub>1-x</sub> ) <sub>2</sub> Pb <sub>3</sub> Br <sub>10</sub>       | 475     | 1.35                   | 100.6                                  | 2019 | [143] |
|        | (PEABr) <sub>x</sub> CsPbBr <sub>3</sub>  | 514     | 12.1                   | 10,270                                 | 2020 | [144] |
|        | PEA <sub>2</sub> (FAPbBr <sub>3</sub> ) <sub>2</sub> PbBr <sub>4</sub>                                    | 532     | 15.4                   | 15,765                                 | 2019 | [145] |
|        | PEA <sub>2</sub> PbBr <sub>4</sub>  | 410     | 0.31                   | 147.6                                  | 2019 | [146] |
|        | P2F8  | 527     | 12.4                   | 5200                                   | 2019 | [147] |
|        | PEA <sub>2</sub> Cs <sub>n-1</sub> Pb <sub>n</sub> Br <sub>3n+1</sub>                                     | 518     | 16.24                  | 30,140                                 | 2020 | [148] |
|        | CsPbCl <sub>0.9</sub> Br <sub>2.1</sub> + PEABr   | 480     | 5.7                    | 3780                                   | 2019 | [84]  |
|        | PEA <sub>2</sub> Cs <sub>n-1</sub> Pb <sub>n</sub> Br <sub>3n+1</sub>                                     | 478     | 6.3                    | ~200                                   | 2020 | [149] |
|        | CsPbBr <sub>3</sub> ; PEACl; YCl <sub>3</sub>   | 485     | 11                     | 9040                                   | 2019 | [120] |
|        | PEA <sub>2</sub> MA <sub>n-1</sub> Pb <sub>n</sub> Br <sub>3n+1</sub>                                     | 515.1   | 9.2 ± 1.43             | 66,000                                 | 2020 | [123] |
|        | PEA <sub>2</sub> Cs <sub>1.6</sub> MA <sub>0.4</sub> Pb <sub>3</sub> Br <sub>10</sub> treated with DPPOCI | 479     | 5.2                    | 468                                    | 2019 | [150] |
|        | 75% PPA + CsPbBr <sub>3</sub>   | /       | 1.87                   | 4700                                   | 2020 | [139] |
|        | PBA <sub>2</sub> Cs <sub>n-1</sub> Pb <sub>n</sub> I <sub>3n+1</sub>                                      | 664     | 13.3                   | 968                                    | 2019 | [122] |
|        | PBA <sub>2</sub> (CsPbBr <sub>3</sub> ) <sub>n-1</sub> PbBr <sub>4</sub>                                  | 514     | 10.4                   | 14,000                                 | 2017 | [151] |
|        | PBA <sub>2</sub> (CsPbI <sub>3</sub> ) <sub>n-1</sub> PbBr <sub>4</sub>                                   | 683     | 7.3                    | /                                      | 2017 | [151] |
|        | PBABr <sub>y</sub> (Cs <sub>0.7</sub> FA <sub>0.3</sub> PbBr <sub>3</sub> )                               | 483     | 9.5                    | 54                                     | 2019 | [152] |

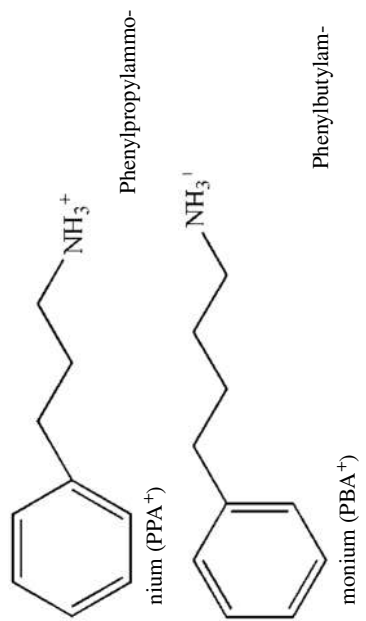
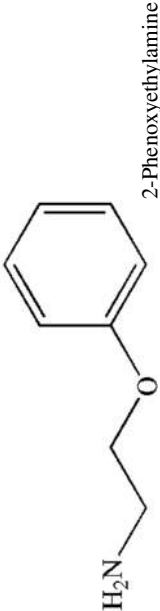
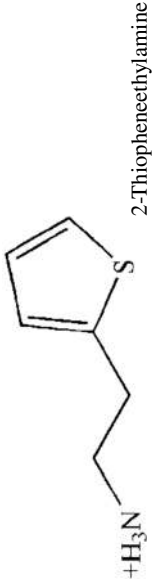
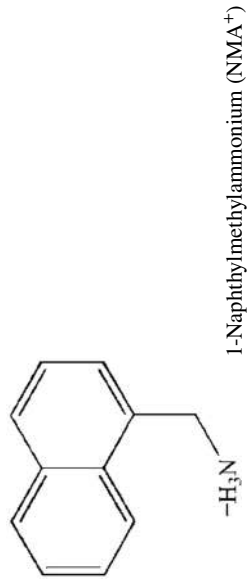


Table 1 (continued)

| Cation  | Emitter material   | EL (nm) | EQE <sub>max</sub> (%) | L <sub>max</sub> (cd m <sup>-2</sup> ) | Year | Refs  |
|---|--|---------|------------------------|--|------|-------|
| <br>H <sub>2</sub> N<br>(POEA)<br>2-Phenoxyethylamine  | POEA(30%); MAPbBr <sub>3</sub>                             | 520     | 2.82                   | 64.2                                   | 2017 | [82]  |
| <br>+H <sub>3</sub> N<br>(TEA <sup>+</sup> )<br>2-Thiopheneethylamine                        | TEA <sub>2</sub> SnI <sub>4</sub>                          | 638     | 0.62                   | 322                                    | 2020 | [30]  |
| <br>+H <sub>3</sub> N<br>(TEA <sup>+</sup> )<br>1-Naphthylmethylammonium (NMA <sup>+</sup> ) | (NMA) <sub>2</sub> (FA) <sub>n-1</sub> PbI <sub>3n+1</sub> | 795     | 20.1                   | /                                      | 2018 | [44]  |
|   | NMA <sub>2</sub> PbBr <sub>4</sub> ; Mn(10%)               | 630     | 0.004                  | /                                      | 2019 | [153] |
|   | NMAI; FABr; PbI <sub>2</sub> (2: 1.9: 2)                   | 780     | 12.7                   | /                                      | 2018 | [91]  |
|   | (NMA) <sub>2</sub> Cs <sub>n-1</sub> PbnI <sub>3n+1</sub>  | 694     | 7.3                    | 732                                    | 2018 | [154] |
|   | 60%NMA + CsPbBr <sub>3</sub>                               | 516     | 6.01                   | 13,200                                 | 2020 | [139] |
|   | (NMA) <sub>2</sub> PbBr <sub>4</sub> ; FABr                | 514     | 14.9                   | 2056                                   | 2018 | [155] |

**Table 1** (continued)

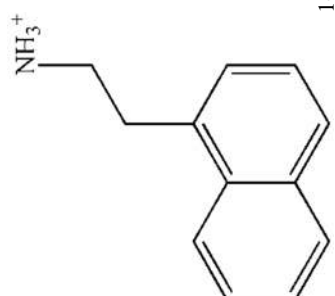
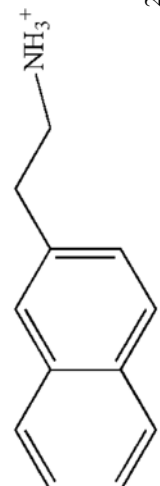
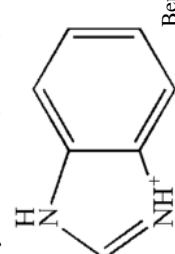



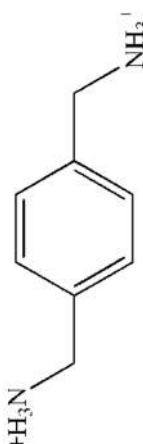
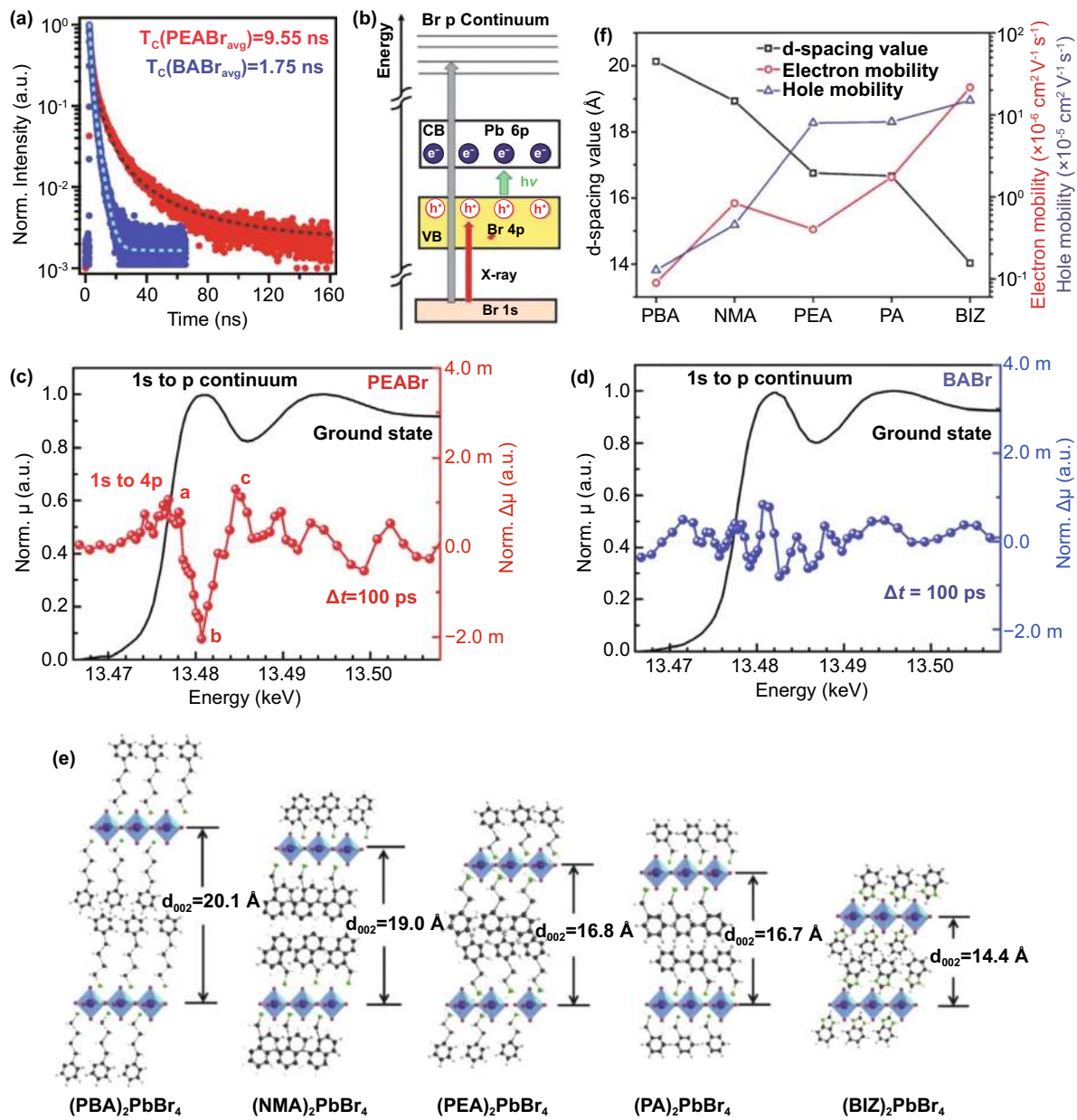
| Cation  | Emitter material  | EL (nm) | EQE <sub>max</sub> (%) | L <sub>max</sub> (cd m <sup>-2</sup> ) | Year | Refs  |
|---|---|---------|------------------------|--|------|-------|
| <br>1-Naphthylethylammonium<br>(1-NEA <sup>+</sup> ) | 60% 1-NEA + CsPbBr <sub>3</sub>   | 509     | 2.45                   | 5200                                   | 2020 | [139] |
| <br>2-Naphthylethylammonium (2-NEA <sup>+</sup> )    | 40% 2-NEA + CsPbBr <sub>3</sub>   | 511     | 1.98                   | 15,000                                 | 2020 | [139] |
| <br>Benzimidazolium (BIZ <sup>+</sup> )              | (BIZ) <sub>2</sub> (FA) <sub>n-1</sub> Pb <sub>n</sub> Br <sub>3n+1</sub> | 535     | 7.7                    | 30,000                                 | 2018 | [124] |
|   | (BIZ) <sub>2</sub> Mn <sub>0.23</sub> Pb <sub>0.77</sub> I <sub>4</sub>   | 575     | 0.045                  | 225                                    | 2019 | [121] |

Table 1 (continued)

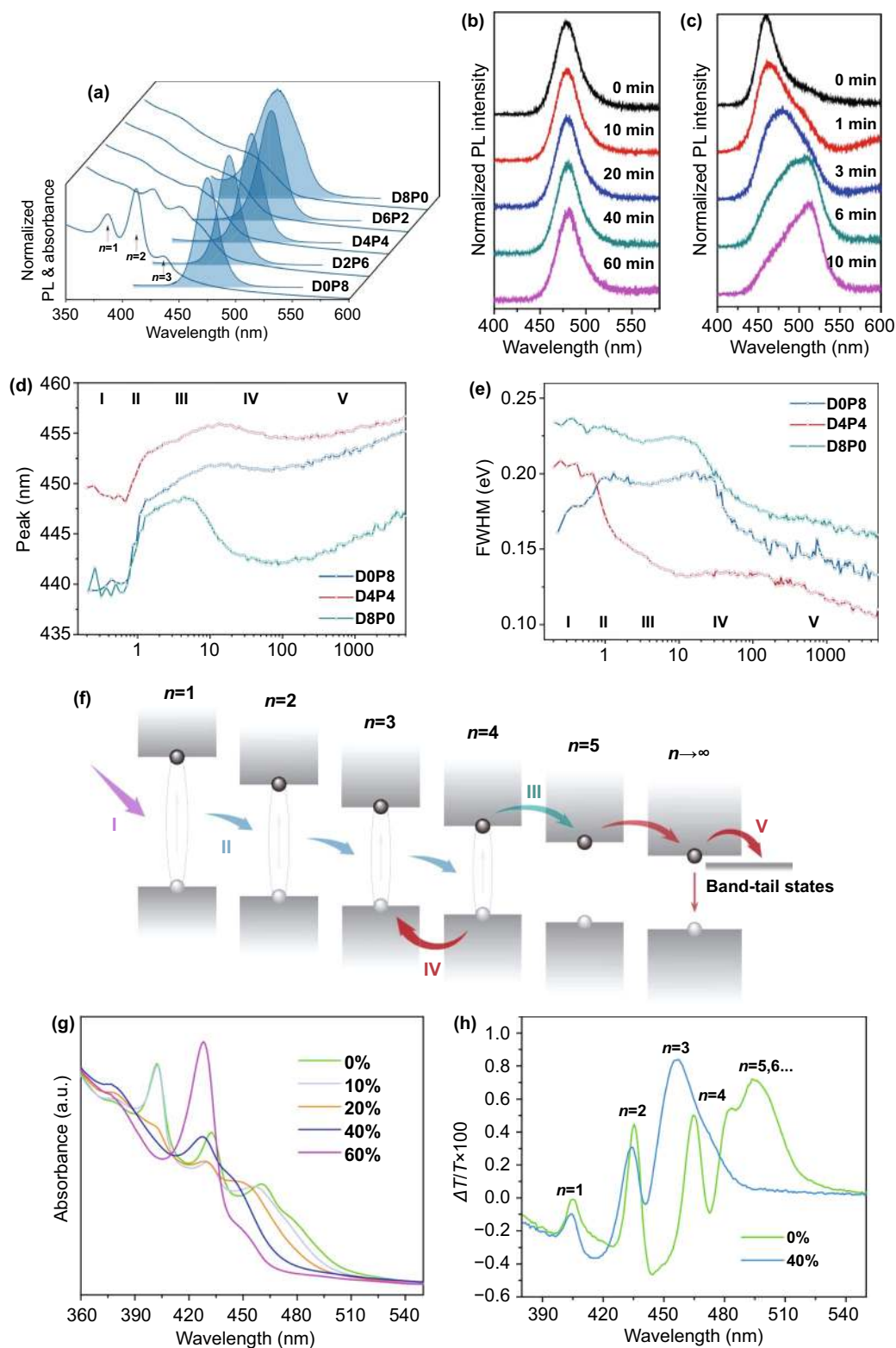
| Cation   | Emitter material  | EL (nm) | EQE <sub>max</sub> (%) | L <sub>max</sub> (cd m <sup>-2</sup> ) | Year | Refs  |
|--|---|---------|------------------------|--|------|-------|
|  NH <sub>3</sub> <sup>+</sup>   | 60% DPPACl + CsPbBr <sub>2</sub> Cl   | 464     | 1.92                   | 442                                    | 2020 | [156] |
|  3,3'-Diphenylpropylammonium (DPPA <sup>+</sup> )                                       | CsBr + PbBr <sub>2</sub> + PDABr <sub>2</sub>   | 490     | 8.5                    | 2257                                   | 2021 | [157] |
|  <sup>-</sup> H <sub>3</sub> N <sup>+</sup> Propane-1,3-diammonium (PDA <sup>2+</sup> ) | (BAB) FA <sub>n-1</sub> Pb <sub>n</sub> X <sub>3n+1</sub>   | 776     | 5.2                    | /                                      | 2019 | [79]  |
|  1,4-Bis(aminomethyl)benzene (BAB)  | (iso-BA <sub>x</sub> PEA <sub>1-x</sub> ) <sub>2</sub> Cs <sub>n-1</sub> Pb <sub>n</sub> (Br <sub>0.7</sub> Cl <sub>0.3</sub> ) <sub>3n+1</sub> (x = 4) | 485     | 7.84                   | 1130                                   | 2020 | [158] |
| PEA <sup>+</sup> + iso-butylammonium (iso-BA <sup>+</sup> )  | IPA/PEA <sub>2</sub> MA/Cs <sub>n-1</sub> Pb <sub>n</sub> Br <sub>3n-1</sub>  | 490     | 1.5                    | 2480                                   | 2018 | [118] |
| PEA <sup>+</sup> + iso-propylammonium (IPA)  | PEA <sub>x</sub> PA <sub>2-x</sub> (CsPbBr <sub>3</sub> ) <sub>n-1</sub> PbBr <sub>4</sub>  | 488     | 7.51                   | 1765                                   | 2020 | [159] |
| PEA <sup>+</sup> + PA <sup>+</sup>   | (BA <sub>0.5</sub> <sup>+</sup> PEA <sub>0.5/2</sub> ) <sub>2</sub> MAPb <sub>2</sub> Br <sub>7</sub>   | 456     | 0.015                  | /                                      | 2020 | [21]  |
| PEA <sup>+</sup> + BA <sup>+</sup>   | P-PDABr <sub>2</sub> + PEABr + CsBr + PbBr <sub>2</sub>   | 465     | 2.6                    | 211                                    | 2019 | [31]  |
| PEA <sup>+</sup> + P-PDA <sup>2+</sup>   | PEA <sub>2</sub> DMA <sub>1.2</sub> Cs <sub>2</sub> Pb <sub>3</sub> Br <sub>11.2</sub>  | 499     | 1.58                   | 7760                                   | 2020 | [160] |
| PEA <sup>+</sup> + dimethylammonium (DMA <sup>+</sup> )  | PEA + NPA + CsBr + PbBr <sub>2</sub>  | 485     | 2.62                   | 1200                                   | 2019 | [161] |
| PEA <sup>+</sup> + N-(2-Bromoethyl)-1,3-propanediamine dihydro (NPA <sup>2+</sup> )  | CsPbCBBr <sub>2</sub> + DPPABr + PEABr  | 470     | 8.8                    | 482                                    | 2020 | [162] |
| PEA <sup>+</sup> + DPPA <sup>+</sup>   | (PBA)(PA)A <sub>n-1</sub> Pb <sub>n</sub> X <sub>3n+1</sub>   | 534     | 15.1                   | 8052                                   | 2020 | [45]  |
| PBA <sup>+</sup> + PA <sup>+</sup>   | PEA <sub>x</sub> PA <sub>2-x</sub> (CsPbBr <sub>3</sub> ) <sub>n-1</sub> PbBr <sub>4</sub> + ABA <sub>2</sub> PbBr <sub>4</sub>                         | 486     | 10.11                  | 513                                    | 2021 | [77]  |
| PEA <sup>+</sup> + PA <sup>+</sup> + ABA <sup>+</sup>  |   |         |                        |  |      |       |



**Fig. 9** **a** Time-resolved PL decay curves for PEABr and BABr thin films. **b** Schematic illustration of bromide (Br) K near edge transitions. The ground-state X-ray absorption spectra as a function of energy and the change in X-ray absorption after 100 ps laser excitation for **c** PEABr and **d** BABr thin films. Copyright 2020 Wiley–VCH Verlag [123]. **e** Schematic representation of the barrier width of  $(\text{PBA})_2\text{PbBr}_4$ ,  $(\text{NMA})_2\text{PbBr}_4$ ,  $(\text{PEA})_2\text{PbBr}_4$ ,  $(\text{PA})_2\text{PbBr}_4$  and  $(\text{BIZ})_2\text{PbBr}_4$  perovskite films. **f** Electron and hole mobilities versus d-spacing value of perovskite films with various organic cations. Copyright 2019 John Wiley and Sons Inc [124]

PEABr is beneficial to the formation of small  $n$  domains. DPPABr and PEABr are mixed in a certain proportion to realize the regulation of quantum well width distribution. Furthermore, the carrier dynamics process is divided into five stages as shown in Fig. 10f. Firstly, photo-generated carriers will be formed in the 2D perovskites after

photoexcitation, resulting in the increase of bleach peak signal. The peak and FWHM fluctuations in Fig. 10d, e are due to the competition of different  $n$  values bleach signals. Then, the carriers transfer rapidly (0.7–1.3 ps) and the bleach peak shifts red. In the third stage, the excitons are decomposed into free carriers and charge transfer occurs,



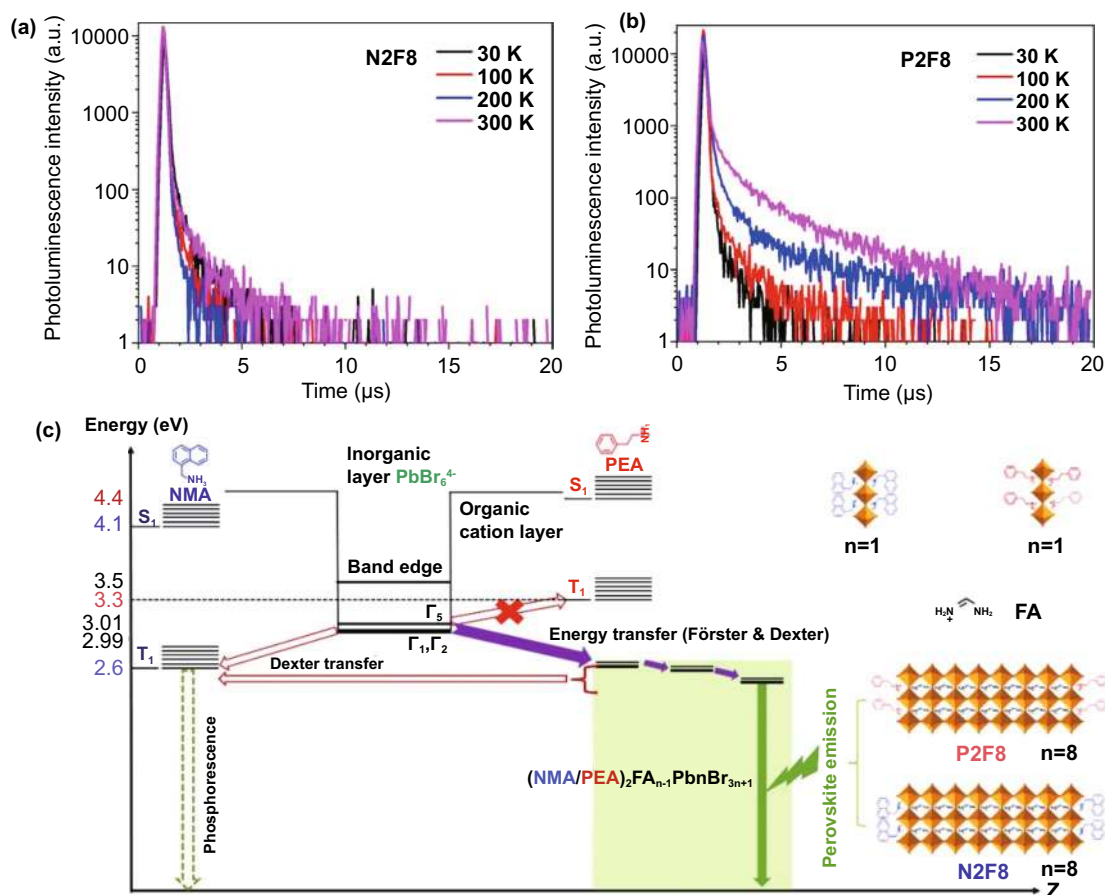
**Fig. 10** **a** Steady-state PL and absorption spectra. PL spectra of **b**  $\text{PEA}_2\text{A}_{1.5}\text{Pb}_{2.5}\text{Br}_{8.5}$  with 40% IPABr and **c**  $\text{MAPbCl}_{1.5}\text{Br}_{1.5}$  under continuous laser radiation for different exposure times. The evolution of **d** peak and **e** FWHM are extracted from the broad bleach peak (425–470 nm) of samples D0P8, D4P4 and D8P0. **f** Schematic diagram of carrier behaviors after excitation. I, carrier formation; II, exciton transfer; III, charge transfer; IV, reverse charge transfer; V, continuous charge transfer and recombination. **g** Absorption spectra of perovskite  $\text{PEA}_2\text{A}_{1.5}\text{Pb}_{2.5}\text{Br}_{8.5}$  with 0–60% IPABr. **h** TA spectra of  $\text{PEA}_2\text{A}_{1.5}\text{Pb}_{2.5}\text{Br}_{8.5}$  with 0 and 40% IPABr. Copyright 2018 Springer Nature [118]. Copyright 2020 Springer Nature [162]

resulting further red shifts of the bleach peak. During the whole process, the FWHM of D4P4 decreases most rapidly (Fig. 10e), indicating the most effective energy transfer and the narrowest distribution of quantum well width. In the fourth stage, due to the blueshift of the bleach peak (about 100 ps) caused by the reverse charge transfer, the energy cannot be concentrated in the effective emission region. Lastly, the free carriers are transferred to the layer with large  $n$  values or band-tail states and recombined through radiative or non-radiative processes. The combination of DPPABr and PEABr not only reduces the small  $n$  value which is not conducive to the emission efficiency, but also shortens the width of quantum well. Likewise, Sargent et al. used IPA and PEA to control the distribution of quantum well width by combining various cations. Their result indicated that the absorption edge shifts blue after inducing IPABr, indicating that the formation of

small  $n$  value phases and large  $n$  value phases is inhibited (Fig. 10g). And Fig. 10h also shows that the existence of large  $n$  phases ( $n = 5, 6, \dots$ ) is not observed after adding 40% IPABr to PEA<sub>2</sub>A<sub>1.5</sub>Pb<sub>2.5</sub>Br<sub>8.5</sub>. In addition, the stability of the device is also enhanced (Fig. 10b, c).

### 3.3.3 Management of Singlet and Triplet Excitons

The management of triplet excitons plays a key role in the design of efficient and stable organic OLEDs. Although the influence of excitons on the performance of PeLEDs is not clear, Adachi et al. used the management strategy of triplet excitons and selected organic cation NMA<sup>+</sup> as the comparison of PEA<sup>+</sup>, which proved the importance of triplet excitons on 2D PeLEDs. It can be seen from Fig. 11a, b that the PL decay curves of (NMA)<sub>2</sub>FA<sub>7</sub>Pb<sub>8</sub>Br<sub>25</sub> (N2F8) and (PEA)<sub>2</sub>FA<sub>7</sub>Pb<sub>8</sub>Br<sub>25</sub> (P2F8) are obviously different. The



**Fig. 11** Photoluminescence decay curves of **a** N2F8 and **b** P2F8. **c** Energy transfer mechanism of quasi-2D perovskites under light excitation. Where S is the singlet state and is the triplet states. Copyright 2019 Springer Nature [147]

decay curve of N2F8 hardly changes under different temperature. However, P2F8 shows fast and slow decay with the increase of temperature, which is due to the thermally activated reverse intersystem crossing (RISC) of triplet excitons. Excitons are formed in 2D perovskites by light excitation. The singlet states transfer rapidly to the large  $n$  domains, but the triplet states are different. As shown in Fig. 11c, PEA<sup>+</sup> has a higher triplet energy level than NMA<sup>+</sup>. And the lowest excited triplet  $T_1$  of PEA<sup>+</sup> is 3.3 eV, which is higher than all triplet energy levels, so PEA<sup>+</sup> can effectively obtain triplet excitons. However, the  $T_1$  of NMA<sup>+</sup> is 2.6 eV, which is lower than the triplet exciton levels  $\Gamma_1$  and  $\Gamma_2$  of [PbBr<sub>6</sub>]<sup>4-</sup>, leading to Dexter energy transfer. Dexter energy transfer will compete with energy transfer in 2D perovskites. The high-efficiency PeLEDs with EQE and current efficiency of 12.4% and 52.1 cd A<sup>-1</sup> are rationally designed by the effectively management of the triplet states [147].

### 3.4 Enhanced Energy Transfer

As mentioned above, compared with 3D perovskite, 2D perovskite has a larger  $E_b$ , and the electrons and holes are effectively confined to enhance the radiation recombination [142]. Moreover, 2D perovskite structure is a common method to construct high-performance PeLEDs. However, due to the random stacking of 2D perovskites, the distribution of  $n$  domains is uneven and multiple emission peaks appear. In addition, small  $n$  phases are formed first in 2D perovskites because of the low formation energy of small  $n$  phases [158]. All of these have negative effects on the energy transfer from small  $n$  domains to large  $n$  ones. In particular, the radiation of  $n=1$  phase belongs to non-radiation recombination, which seriously affects the performance of PeLEDs. Yang et al. introduced methanesulfonate (MES) to reconstruct the phase distribution of perovskite and promote the energy transfer from small  $n$  phase to large  $n$  one. The density functional theory (DFT) calculation shows that SO<sub>3</sub><sup>-</sup> in MES tends to form a strong force with organic cation BA<sup>+</sup>, and the charge redistribution between them is 0.84 e (electron), which is greater than that between BA<sup>+</sup> and Br<sup>-</sup> (0.70 e) (Fig. 12a). The existence of hydrogen bonds increases large  $n$  domains, which can regulate the crystallization kinetics. In Fig. 12b, the exciton resonance at GSB <sub>$n=2$</sub>  still exists after long-time excitation at 101 ps. However, the exciton resonance at

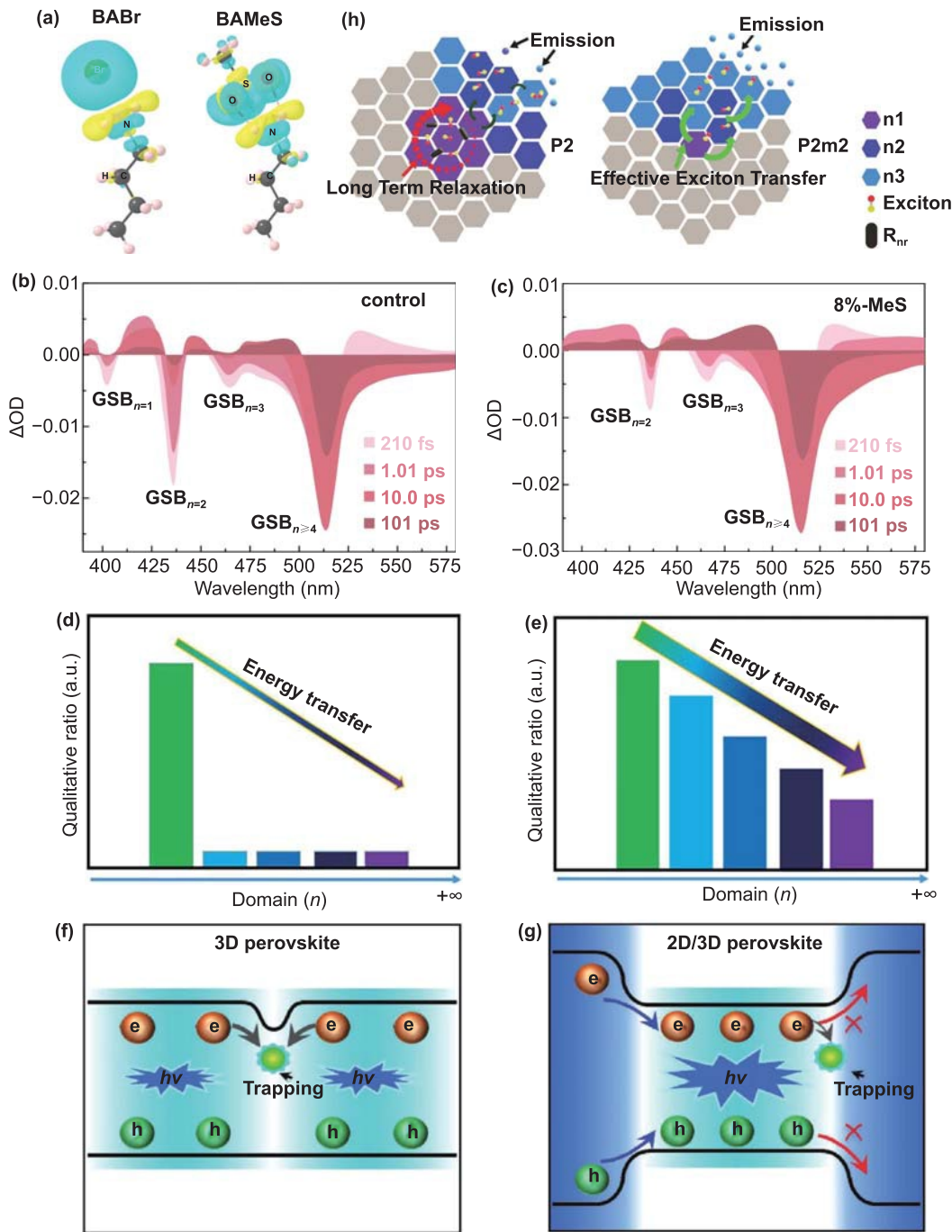
GSB <sub>$n=2$</sub>  is not found in the 8%-MES films (Fig. 12c). The reason resulting in the noticeable difference is due to the effect of effective energy transfer. It is gratifying that the exciton resonance of GSB <sub>$n=1$</sub>  is not found in the 8%-MES films. The introduction of MES successfully inhibits the formation of small  $n$  phases. Eventually, quasi-2D green PeLED with EQE up to 20.5% is obtained [134]. Ning et al. achieved high carrier transfer efficiency based on DJ structure by adjusting the ratio of BAB to FA in (BAB)FA <sub>$n-1$</sub> Pb <sub>$n$</sub> X <sub>$3n+1$</sub>  ( $X=Br, I$ ). As shown in Fig. 12d, e, the peak intensity of BAB25 in the large  $n$  domain is about twice that of BAB33 [79]. As we all known, many defects in 3D perovskites are not conducive to radiative recombination (Fig. 12f). Zeng et al. used the 2D/3D perovskite structure to make the energy levels connected and enhance the energy transfer. The formation of energy level cascade channels makes the energy transfer from the wide bandgap to the narrow bandgap (Fig. 12g), which enhances the radiative recombination efficiency. Although the organic ligands of 2D perovskites do not contribute to the charge transfer, the free charge diffusion is inhibited in 3D perovskites, which can just combine with the opposite charge. The coordination effect of the above two factors has successfully increased the EQE value by about 5 times, and the stability has also been greatly improved [163]. By introducing [1,4-Bis(aminomethyl)benzene bromide (P-PDABr<sub>2</sub>)], the exciton shifts rapidly from small  $n$  domains to large ones (Fig. 12h).

## 4 Current Challenges Ahead in 2D PeLEDs

### 4.1 Improving Efficiency of Blue 2D PeLEDs

Since 2014, the largest EQEs of green and red PeLEDs have exceeded 20%, and have made great achievements [164–170]. However, as one of the primary colors of high-definition displays [171], the development of blue PeLEDs is quite slow, far behind red and green PeLEDs. As shown in Fig. 13a. The universal strategy for preparing blue emission is to control the mixed halogen anions so that achieve tuning of continuous bandgap by adding chlorine (Cl) to the bromide (Br)-based perovskites and modulating the proportion of halogen ions (Fig. 13b, c) [84, 172]. But the spectral shift of these mixed perovskites usually occurs under different operating voltages, which is due to the migration and

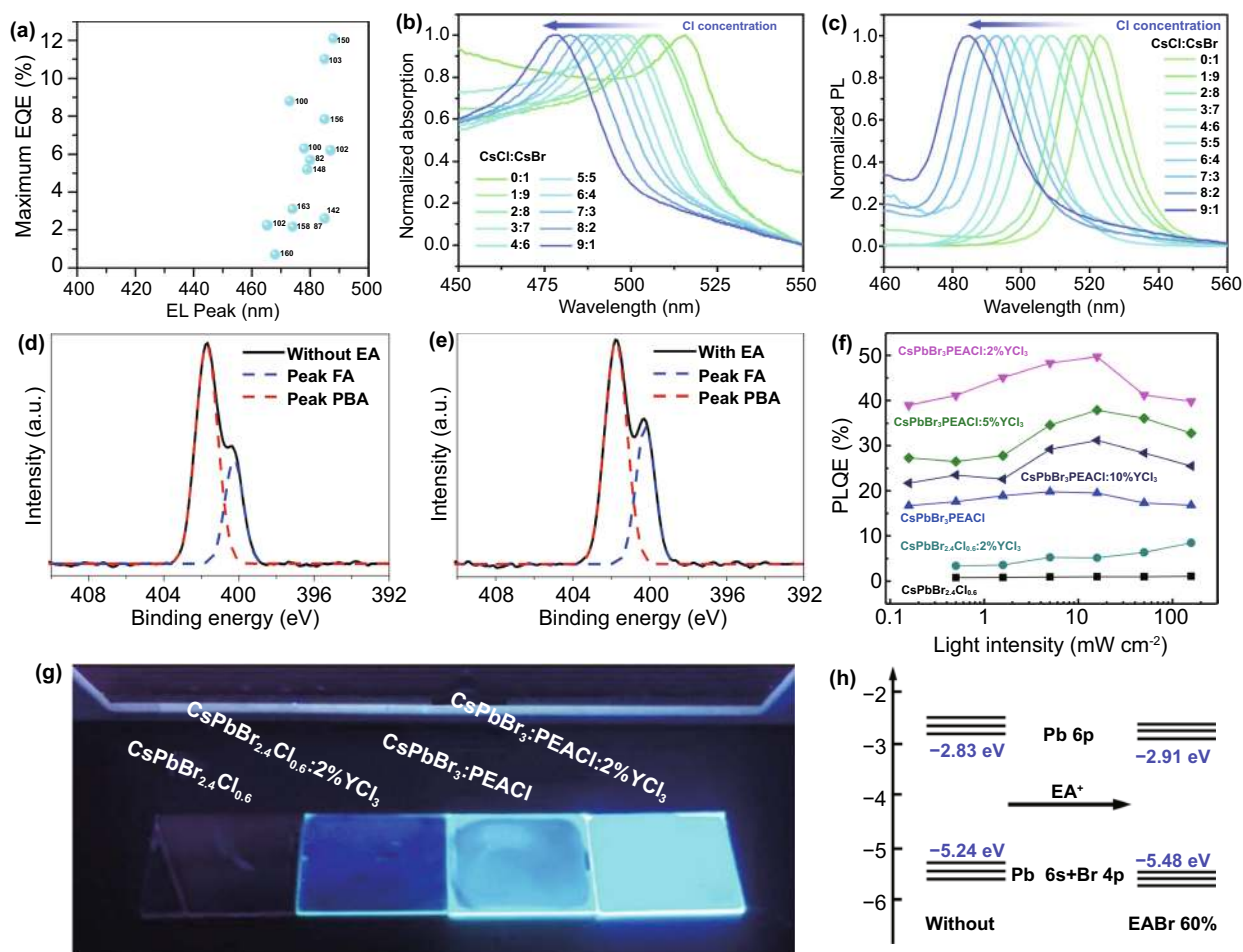




**Fig. 12** **a** Hydrogen bond calculations. Differential charge density diagrams of BABr and BAMEs (where isosurface value is  $0.0015 \text{ eV \AA}^{-3}$ ; cyan is charge accumulation; yellow is charge depletion). TA spectra at selected timescales of the **b** control and **c** 8%-MES perovskite films. Copyright 2021 Springer Nature [134]. The energy transfer process of **d** BAB33 and **e** BAB25 perovskite films was studied. Copyright 2019 American Association for the Advancement of Science [79]. Comparison of **f** 3D and **g** 2D/3D perovskite film carrier recombination. Copyright 2020 Wiley-VCH Verlag [163]. **h** Domain distribution, exciton transfer and emission properties of P2 and P2m2 films. Copyright 2019 Wiley-Blackwell [31]

segregation of mixed halides [173, 174]. In addition, different metal ions such as  $\text{Mn}^{2+}$ ,  $\text{Al}^{3+}$ ,  $\text{Cu}^{2+}$  and  $\text{Zn}^{2+}$  are doped

into the B site to adjust the conduction band [175–178]. Unfortunately, the impurity energy levels induced by metal



**Fig. 13** **a** Comparison of EQE values of 2D perovskites blue LEDs with EL peak in the range of 400–500 nm. **b** Normalized absorption and **c** photoluminescence spectra of CsPbCl<sub>x</sub>Br<sub>3-x</sub> thin films with different molar ratios of CsCl to CsBr. Copyright 2019 Springer Nature [84]. High-resolution N 1s XPS spectra of the perovskite films without **d** and **e** with EA treatment. Copyright 2019 Springer Nature [152]. **f** A photograph of the perovskite films under the ultraviolet lamp. **g** Power-dependent PLQEs of films with different compositions. Copyright 2019 Springer Nature [120]. **h** Diagram of energy levels change of quasi-2D perovskite in Pb 6p and (Pb 6s + Br 4p) orbitals with EA + insertion. Copyright 2020 Springer Nature [141]

ions are disadvantageous to radiative recombination. At present, it is also an important strategy to achieve blue emission by inserting large organic cations into 3D perovskites. Ma and co-workers not only introduced PEABr into CsPbX<sub>3</sub>, but also rearranged the 2D perovskite phase distribution with NaBr, which reduced the formation of a small *n* domain (*n* = 1) dominated by non-radiative recombination and increased PLQY from 39 to 67%. The sky-blue PeLED with EQE up to 11.7% was obtained [78]. However, the charge transport capacity of 2D perovskites is poor due to the organic compounds acting as spacer cations. Jin et al. used ethyl acetate (EA) as the anti-solvent, which was beneficial to the dissolution of PBABr, and would not damage

the emission layer and the underlying layer. As shown in the high-resolution N 1s XPS spectra, EA changed the ratio of PBA<sup>+</sup> and FA<sup>+</sup> (Fig. 13d, e) [152]. Huang et al. introduced PEACl into CsPbBr<sub>3</sub> to facilitate the formation of layered perovskites, and further doped YCl<sub>3</sub>, resulting in a qualitative leap in the PLQE of the films, from 1.1 to 49.7% (Fig. 13f). CsPbBr<sub>3</sub>:PEACl:2%YCl<sub>3</sub> exhibits the brightest luminescence under the ultraviolet lamp (Fig. 13g). However, the existence of yttrium on CsPbBr<sub>3</sub> grain increases the bandgap and forces the radiative recombination of carriers in CsPbBr<sub>3</sub>. The sky-blue PeLED with a maximum brightness of 9040 cd m<sup>-2</sup> and EQE of 11.0% are prepared [120]. The above efficient perovskite blue LEDs mainly focus on

the modification of organic cations. You et al. used  $\text{EA}^+$  to replace Cs in  $\text{PEA}_2(\text{CsPbBr}_3)_2\text{PbBr}_4$  at A site, which makes the maximum valence band of the 2D perovskite moves down and the bandgap increase (Fig. 13h). So far, this may be the highest efficiency of sky-blue LED (12.1%). Moreover, the device shows excellent stability and can survive for as long as 1 h without encapsulation in nitrogen [141]. Although 2D perovskite blue LEDs have made great progress, their applications in full-color display and white lighting are still far away, which is a huge challenge.

#### 4.2 Enhanced Stability of 2D PeLEDs

At present, some excellent works have reported more than the EQEs of 2D PeLEDs exceed 20%. Unfortunately, the stability of 2D PeLEDs is poor, which is a stumbling block in practical application. As we all know,  $T_{50}$  is one of the important parameters to evaluate the stability of LEDs. However, at the low luminance of  $100 \text{ cd m}^{-2}$ , the  $T_{50}$  values of most blue 2D PeLEDs reported so far are tens of minutes [120, 152, 161], some even tens of seconds [78, 141], which are far from those of OLED and QD LEDs. Compared with perovskite solar cells, PeLEDs need to work in higher applied electric field. Ion migration is the main factor leading to poor stability of 2D PeLEDs. To enhance the stability of PeLEDs, it is necessary to effectively suppress ion migration. Because ion migration mainly occurs at grain boundaries, preventing ion migration along grain boundaries is a feasible way to suppress ion migration. Lee et al. designed proton-transfer-induced 2D perovskite formation while retaining 3D perovskite. Compared with  $\text{MA}^+$ , due to the  $\pi - \pi$  interaction and steric repulsion of Benzylamine cation ( $\text{BnA}^+$ ), the reorientation rate is significantly reduced and the ion migration along grain boundaries is effectively suppressed [179]. Furthermore, the decomposition of organic cations a voltage bias is one of the reasons for the instability of 2D PeLEDs. Snaith et al. found that phenylethylammonium bromide (PEABr) greatly improves the efficiency of  $\text{CsPbBr}_3$  LEDs, but PEABr will decompose and produce mobile ions, which will move to ETL, eventually leading to the charge imbalance of the device [144]. In RP phase, the adjacent inorganic octahedral slabs have an inherent dissociation tendency, which also leads to the decomposition of perovskites, and the organic cations are connected by weak van der Waals force. Therefore, enhancing the interaction

between large organic cations and octahedral slabs is beneficial to improve the stability of 2D PeLEDs. The octahedral slabs of DJ phase are bridged by diamine cations, and the interaction force is stronger than that of monoamine cations of RP phase [157]. Ning et al. used 1,4-bis(aminomethyl)benzene (BAB) as bridging molecules to obtain a 2D PeLED with  $T_{50}$  lifetime up to 100 h, which is almost two orders of magnitude longer than that of RP phase (PEA as organic spacer cation) [79].

In addition, the stability of PeLEDs is also related to the thermal stability of the material. Under the continuous operating voltage, the Joule heat causes the perovskite interface to be heated, leading to degradation. Most of the 2D perovskite films are easy to transform into mixed 2D/3D phases when heated [180]. Moreover, the efficiency of the devices will be adversely affected if the annealing temperature is too high and the annealing time is too long [181].

#### 4.3 Toxicity Reduction of 2D PeLEDs

Most of the researches on 2D perovskite optoelectronic devices are mainly based on lead-based perovskites at the moment. Although the lead content meets the standard of commercial products, lead-based perovskite is easily soluble in water. If the encapsulant material is damaged, lead leakage occurs and seeps into the water, which will cause serious pollution to the environment. In recent years, lead-free tin-based perovskite has attracted people's attention [31, 182]. Unfortunately,  $\text{Sn}^{2+}$  is easily oxidized to  $\text{Sn}^{4+}$ . Moreover, the crystallization rate of Sn-based perovskite is faster than that of Pb-based perovskite, resulting in more defects. The films are prone to non-radiative recombination caused by defects, which seriously affects the performance of devices. Sargent et al. introduced liquid reductant  $\text{H}_3\text{PO}_2$  into the precursor solution to inhibit the oxidation of  $\text{Sn}^{2+}$ , and obtained red LED with maximum brightness of  $70 \text{ cd m}^{-2}$  and EQE of 0.3% [183]. Soon after, they developed a new strategy, using valeric acid to slow down the Sn-based crystallization rate and avoid the formation of  $\text{Sn}^{4+}$ . Thus, the lead-free red PeLED with the longest half-life and the highest EQE (5%) was obtained [114]. Dou et al. used 7-(thiophen-2-yl)benzothiadiazol-4-yl)-[2,2'-bithiophen]-5-yl)ethylammonium iodide (BTmI) as the barrier layers to display a pure red Sn-based PeLED with a luminance of  $3466 \text{ cd m}^{-2}$  and a working stability of more than 150 h [184]. (111)-oriented 2D



perovskites have also been used as LEDs, but they all show unsatisfactory efficiency. The first example using  $\text{Cs}_3\text{Sb}_2\text{I}_9$  as the emitting layer was reported by Chu et al. The wavelength of  $\text{Cs}_3\text{Sb}_2\text{I}_9$  is controlled by the vapor anion exchange method. The device shows an average radiance of  $0.012 \text{ W sr}^{-1} \text{ m}^{-2}$  at 6 V [185]. Shan and his colleagues reported lead-free  $\text{Cs}_3\text{Sb}_2\text{Br}_9$  with EQE of  $\sim 0.206\%$ , which is the shortest wavelength PeLED known to us [186]. Even though the performances of lead-free PeLEDs are far from that of lead-based perovskite, there is a great room for development.

## 5 Conclusions and Outlook

In this review, we summarize the applications of 2D perovskites in LEDs in recent years, mainly RP perovskites. Compared with typical 3D  $\text{ABX}_3$ , 2D perovskites have natural quantum well structures, larger  $E_b$  and better ambient stability. The structure of 2D perovskites can be regarded as the periodic splitting of 3D perovskites along (100), (110) and (111) planes by organic cations. RP perovskites belong to (100)-oriented 2D perovskites. Here, we analyze and compare the structures of 2D perovskites with different orientations. In this direction, more and more new members have been found, increasing members of halide perovskite group. Moreover, 2D perovskites have many excellent properties, such as convenient control of the width of quantum wells, formation of dense films and ultra-fast energy transfer, which shows great potential in the field of optoelectronic devices. However, there are many types of organic spacers, so how choose organic cations correctly is the key to promote the development of PeLEDs. The effects of steric hindrance and alkyl chain length on the performance of the devices are briefly described. Although many alkylamines or aromatic amines have been explored as spacers, there is still a lot of space to expand the 2D perovskites family, which is helpful to understand the 2D perovskites comprehensively and to grasp the influence of perovskites structures and properties on device performance fundamentally.

Unfortunately, the introduction of organic cations also has negative effects. Due to the rapid nucleation, 2D perovskites usually contain many different  $n$  values, resulting in multipeak emission, which is fatal for high color purity display. Therefore, the accurate control of phase purity is one of the key factors in the design of efficient

and stable PeLEDs. Although some promising results have been achieved, there is still a long way to go for large-scale productions of films. It is necessary to further study the nucleation and growth mechanism of 2D perovskites. In addition, as an emerging technology, the stability of 2D PeLEDs is also a big obstacle to their practical applications. In 2D perovskite materials, although large organic cations can improve the humidity resistance of films, the stability of devices is still threatened by ion migration, thermal instability and interface instability. Currently, passivation of surface defects and control of crystal growth rate is often used to alleviate the instability of perovskites phase. How to obtain long-term stable and efficient 2D PeLEDs needs further research.

In summary, due to the unique photoelectric performance of quasi-2D, PeLEDs have experienced a blowout type development in just seven years. It has the potential to surpass OLEDs and QD LEDs and is expected to be used in next-generation displays and lighting equipment. Although remarkable achievements have been made, many problems still remain unsolved. We hope that this review will provide a comprehensive summary for society to deepen the understanding of 2D PeLEDs.

**Acknowledgements** This work was supported by the National Natural Science Foundation of China (Grant No. 21661010) and the Guangxi Natural Science Foundation (Grant No. 2017GXNSFGA198005).

**Open Access** This article is licensed under a Creative Commons Attribution 4.0 International License, which permits use, sharing, adaptation, distribution and reproduction in any medium or format, as long as you give appropriate credit to the original author(s) and the source, provide a link to the Creative Commons licence, and indicate if changes were made. The images or other third party material in this article are included in the article's Creative Commons licence, unless indicated otherwise in a credit line to the material. If material is not included in the article's Creative Commons licence and your intended use is not permitted by statutory regulation or exceeds the permitted use, you will need to obtain permission directly from the copyright holder. To view a copy of this licence, visit <http://creativecommons.org/licenses/by/4.0/>.

## References

1. X. Li, J.M. Hoffman, M.G. Kanatzidis, The 2D halide perovskite rulebook: how the spacer influences everything from the structure to optoelectronic device efficiency. *Chem. Rev.* **121**(4), 2230–2291 (2021). <https://doi.org/10.1021/acs.chemrev.0c01006>

2. K. Yang, F. Li, H. Hu, T. Guo, T.W. Kim, Surface engineering towards highly efficient perovskite light-emitting diodes. *Nano Energy* **65**, 104029 (2019). <https://doi.org/10.1016/j.nanoen.2019.104029>
3. J.E. Jeong, J.H. Park, C.H. Jang, M.H. Song, H.Y. Woo, Multifunctional charge transporting materials for perovskite light-emitting diodes. *Adv. Mater.* **32**(51), 2002176 (2020). <https://doi.org/10.1002/adma.202002176>
4. T.H. Han, S. Tan, J. Xue, L. Meng, J.W. Lee et al., Interface and defect engineering for metal halide perovskite optoelectronic devices. *Adv. Mater.* **31**(47), e1803515 (2019). <https://doi.org/10.1002/adma.201803515>
5. R. Zeng, K. Bai, Q. Wei, T. Chang, J. Yan et al., Boosting triplet self-trapped exciton emission in Te(IV)-doped Cs<sub>2</sub>SnCl<sub>6</sub> perovskite variants. *Nano Res.* **14**(5), 1551–1558 (2021). <https://doi.org/10.1007/s12274-020-3214-x>
6. L. Chu, W. Ahmad, W. Liu, J. Yang, R. Zhang et al., Lead-free halide double perovskite materials: a new superstar toward green and stable optoelectronic applications. *Nano-Micro Lett.* **11**(1), 16 (2019). <https://doi.org/10.1007/s40820-019-0244-6>
7. W. Liu, N. Liu, S. Ji, H. Hua, Y. Ma et al., Perfection of perovskite grain boundary passivation by rhodium incorporation for efficient and stable solar cells. *Nano-Micro Lett.* **12**(1), 119 (2020). <https://doi.org/10.1007/s40820-020-00457-7>
8. X. Zhou, L. Qiu, R. Fan, J. Zhang, S. Hao et al., Heterojunction incorporating perovskite and microporous metal-organic framework nanocrystals for efficient and stable solar cells. *Nano-Micro Lett.* **12**(1), 80 (2020). <https://doi.org/10.1007/s40820-020-00417-1>
9. M. Shahiduzzaman, M.I. Hossain, S. Visal, T. Kaneko, W. Qarony et al., Spray pyrolyzed TiO<sub>2</sub> embedded multi-layer front contact design for high-efficiency perovskite solar cells. *Nano-Micro Lett.* **13**(1), 36 (2021). <https://doi.org/10.1007/s40820-020-00559-2>
10. S. Fu, X. Li, L. Wan, W. Zhang, W. Song et al., Effective surface treatment for high-performance inverted CsPbI<sub>2</sub>Br perovskite solar cells with efficiency of 15.92%. *Nano-Micro Lett.* **12**(1), 170 (2020). <https://doi.org/10.1007/s40820-020-00509-y>
11. K. Ji, M. Anaya, A. Abfalterer, S.D. Stranks, Halide perovskite light-emitting diode technologies. *Adv. Opt. Mater.* (2021). <https://doi.org/10.1002/adom.202002128>
12. B. Ke, R. Zeng, Z. Zhao, Q. Wei, X. Xue et al., Homo- and heterovalent doping-mediated self-trapped exciton emission and energy transfer in Mn-doped Cs<sub>2</sub>Na<sub>1-x</sub>Ag<sub>x</sub>BiCl<sub>6</sub> double perovskites. *J. Phys. Chem. Lett.* **11**(1), 340–348 (2020). <https://doi.org/10.1021/acs.jpcclett.9b03387>
13. J. Huang, T. Chang, R. Zeng, J. Yan, Q. Wei et al., Controlled structural transformation in Sb-doped indium halides A<sub>3</sub>InCl and A<sub>2</sub>InCl<sub>5</sub>•H<sub>2</sub>O yields reversible green-to-yellow emission switch. *Adv. Opt. Mater.* (2021). <https://doi.org/10.1002/adom.202002267>
14. R. Zeng, L. Zhang, Y. Xue, B. Ke, Z. Zhao et al., Highly efficient blue emission from self-trapped excitons in stable Sb<sup>3+</sup>-doped Cs<sub>2</sub>NaInCl<sub>6</sub> double perovskites. *J. Phys. Chem. Lett.* **11**(6), 2053–2061 (2020). <https://doi.org/10.1021/acs.jpcclett.0c00330>
15. K. Liao, C. Li, L. Xie, Y. Yuan, S. Wang et al., Hot-casting large-grain perovskite film for efficient solar cells: film formation and device performance. *Nano-Micro Lett.* **12**(1), 1–22 (2020). <https://doi.org/10.1007/s40820-020-00494-2>
16. X. Wang, L. Wang, T. Shan, S. Leng, H. Zhong et al., Low-temperature aging provides 22% efficient bromine-free and passivation layer-free planar perovskite solar cells. *Nano-Micro Lett.* **12**(1), 84 (2020). <https://doi.org/10.1007/s40820-020-00418-0>
17. P. Fu, S. Hu, J. Tang, Z. Xiao, Material exploration via designing spatial arrangement of octahedral units: a case study of lead halide perovskites. *Front. Optoelect.* (2021). <https://doi.org/10.1007/s12200-021-1227-z>
18. C. Sun, Y. Jiang, M. Cui, L. Qiao, J. Wei et al., High-performance large-area quasi-2D perovskite light-emitting diodes. *Nat. Commun.* **12**(1), 2207 (2021). <https://doi.org/10.1038/s41467-021-22529-x>
19. D. Wang, D. Wu, D. Dong, W. Chen, J. Hao et al., Polarized emission from CsPbX<sub>3</sub> perovskite quantum dots. *Nanoscale* **8**(22), 11565–11570 (2016). <https://doi.org/10.1039/c6nr01915c>
20. H. Shi, X. Zhang, X. Sun, X. Zhang, Phonon mode transformation in size-evolved solution-processed inorganic lead halide perovskite. *Nanoscale* **10**(21), 9892–9898 (2018). <https://doi.org/10.1039/c7nr09101j>
21. T.L. Leung, H.W. Tam, F. Liu, J. Lin, A.M.C. Ng et al., Mixed spacer cation stabilization of blue-emitting n = 2 Ruddlesden-Popper organic-inorganic halide perovskite films. *Adv. Opt. Mater.* **8**(4), 1901679 (2020). <https://doi.org/10.1002/adom.201901679>
22. H.L. Wells, On the caesium- and the potassium-lead halides. *Am. J. Sci.* **s3-45**(266), 121–134 (1893). <https://doi.org/10.2475/ajs.s3-45.266.121>
23. D. Weber, CH<sub>3</sub>NH<sub>3</sub>PbX<sub>3</sub>, ein Pb(II)-System mit kubischer Perovskitstruktur/CH<sub>3</sub>NH<sub>3</sub>PbX<sub>3</sub>, a Pb(II)-system with cubic perovskite structure. *Zeitschrift für Naturforschung B* **33**(12), 1443–1445 (1978). <https://doi.org/10.1515/znb-1978-1214>
24. D.B. Mitzi, C.A. Feild, W.T.A. Harrison, A.M. Guloy, Conducting tin halides with a layered organic-based perovskite structure. *Nature* **369**(6480), 467–469 (1994). <https://doi.org/10.1038/369467a0>
25. D.B. Mitzi, S. Wang, C.A. Feild, C.A. Chess, A.M. Guloy, Conducting layered organic-inorganic halides containing <110>-oriented perovskite sheets. *Science* **267**(5203), 1473–1476 (1995). <https://doi.org/10.1126/science.267.5203.1473>
26. A. Kojima, K. Teshima, Y. Shirai, T. Miyasaka, Organometal halide perovskites as visible-light sensitizers for photovoltaic cells. *J. Am. Chem. Soc.* **131**(17), 6050–6051 (2009). <https://doi.org/10.1021/ja809598r>
27. Z. Tan, R.S. Moghaddam, M.L. Lai, P. Docampo, R. Higler et al., Bright light-emitting diodes based on organometal



- halide perovskite. *Nat. Nanotechnol.* **9**(9), 687–692 (2014). <https://doi.org/10.1038/nnano.2014.149>
28. L. Mao, C.C. Stoumpos, M.G. Kanatzidis, Two-dimensional hybrid halide perovskites: principles and promises. *J. Am. Chem. Soc.* **141**(3), 1171–1190 (2019). <https://doi.org/10.1021/jacs.8b10851>
29. C. Lan, Z. Zhou, R. Wei, J.C. Ho, Two-dimensional perovskite materials: from synthesis to energy-related applications. *Mater. Today Energy* **11**, 61–82 (2019). <https://doi.org/10.1016/j.mtener.2018.10.008>
30. Z. Wang, F. Wang, B. Zhao, S. Qu, T. Hayat et al., Efficient two-dimensional tin halide perovskite light-emitting diodes via a spacer cation substitution strategy. *J. Phys. Chem. Lett.* **11**(3), 1120–1127 (2020). <https://doi.org/10.1021/acs.jpcclett.9b03565>
31. S. Yuan, Z.K. Wang, L.X. Xiao, C.F. Zhang, S.Y. Yang et al., Optimization of low-dimensional components of quasi-2D perovskite films for deep-blue light-emitting diodes. *Adv. Mater.* **31**(44), e1904319 (2019). <https://doi.org/10.1002/adma.201904319>
32. Y. Huang, Y. Li, E.L. Lim, T. Kong, Y. Zhang et al., Stable layered 2D perovskite solar cells with an efficiency of over 19% via multifunctional interfacial engineering. *J. Am. Chem. Soc.* **143**(10), 3911–3917 (2021). <https://doi.org/10.1021/jacs.0c13087>
33. P. Liu, N. Han, W. Wang, R. Ran, W. Zhou, Z. Shao, High-quality Ruddlesden-Popper perovskite film formation for high-performance perovskite solar cells. *Adv. Mater.* **33**(10), e2002582 (2021). <https://doi.org/10.1002/adma.202002582>
34. H. Kim, M. Pei, Y. Lee, A.A. Sultanto, S. Paek et al., Self-crystallized multifunctional 2D perovskite for efficient and stable perovskite solar cells. *Adv. Funct. Mater.* **30**(19), 1910620 (2020). <https://doi.org/10.1002/adfm.201910620>
35. J. Lee, Z. Dai, T. Han, C. Choi, S. Chang et al., 2D perovskite stabilized phase-pure formamidinium perovskite solar cells. *Nat. Commun.* **9**(1), 3010–3021 (2018). <https://doi.org/10.1038/s41467-018-05454-4>
36. J. Wang, J. Li, S. Lan, C. Fang, H. Shen et al., Controllable growth of centimeter-sized 2D perovskite heterostructures for highly narrow dual-band photodetectors. *ACS Nano* **13**(5), 5473–5484 (2019). <https://doi.org/10.1021/acsnano.9b00259>
37. F. Zhou, I. Abdelwahab, K. Leng, K.P. Loh, W. Ji, 2D perovskites with giant excitonic optical nonlinearities for high-Performance sub-bandgap photodetection. *Adv. Mater.* **31**(48), e1904155 (2019). <https://doi.org/10.1002/adma.201904155>
38. C. Qin, A. Sandanayaka, C. Zhao, T. Matsushima, D. Zhang et al., Stable room-temperature continuous-wave lasing in quasi-2D perovskite films. *Nature* **585**(7823), 53–57 (2020). <https://doi.org/10.1038/s41586-020-2621-1>
39. H. Zhang, Q. Liao, Y. Wu, Z. Zhang, Q. Gao et al., 2D Ruddlesden-Popper perovskites microring laser array. *Adv. Mater.* **30**(15), e1706186 (2018). <https://doi.org/10.1002/adma.201706186>
40. S. Chou, R. Ma, Y. Li, F. Zhao, K. Tong et al., Transparent perovskite light-emitting touch-responsive device. *ACS Nano* **11**(11), 11368–11375 (2017). <https://doi.org/10.1021/acsnano.7b05935>
41. M. Yuan, L.N. Quan, R. Comin, G. Walters, R. Sabatini et al., Perovskite energy funnels for efficient light-emitting diodes. *Nat. Nanotechnol.* **11**(10), 872–877 (2016). <https://doi.org/10.1038/nnano.2016.110>
42. N. Wang, L. Cheng, R. Ge, S. Zhang, Y. Miao et al., Perovskite light-emitting diodes based on solution-processed self-organized multiple quantum wells. *Nat. Photonics* **10**(11), 699–704 (2016). <https://doi.org/10.1038/nphoton.2016.185>
43. Y. Liu, Z. Yu, S. Chen, J.H. Park, E.D. Jung et al., Boosting the efficiency of quasi-2D perovskites light-emitting diodes by using encapsulation growth method. *Nano Energy* **80**, 105511 (2021). <https://doi.org/10.1016/j.nanoen.2020.105511>
44. B. Zhao, S. Bai, V. Kim, R. Lamboll, R. Shivanna et al., High-efficiency perovskite-polymer bulk heterostructure light-emitting diodes. *Nat. Photonics* **12**(12), 783–789 (2018). <https://doi.org/10.1038/s41566-018-0283-4>
45. F. Meng, X. Liu, Y. Chen, X. Cai, M. Li et al., Co-interlayer engineering toward efficient green quasi-two-dimensional perovskite light-emitting diodes. *Adv. Funct. Mater.* **30**(19), 1910167 (2020). <https://doi.org/10.1002/adfm.201910167>
46. C. Liang, D. Zhao, Y. Li, X. Li, S. Peng et al., Ruddlesden-Popper perovskite for stable solar cells. *Energy Environ. Mater.* **1**(4), 221–231 (2018). <https://doi.org/10.1002/eam2.12022>
47. O. Nazarenko, M.R. Kotyrba, S. Yakunin, M. Aebli, G. Raino et al., Guanidinium-formamidinium lead iodide: a layered perovskite-related compound with red luminescence at room temperature. *J. Am. Chem. Soc.* **140**(11), 3850–3853 (2018). <https://doi.org/10.1021/jacs.8b00194>
48. C. Ortiz Cervantes, P. Carmona Monroy, D. Solis Ibarra, Two-dimensional halide perovskites in solar cells: 2D or not 2D? *Chemosuschem* **12**(8), 1560–1575 (2019). <https://doi.org/10.1002/cssc.201802992>
49. T. Hu, M.D. Smith, E.R. Dohner, M.J. Sher, X. Wu et al., Mechanism for broadband white-light emission from two-dimensional (110) hybrid perovskites. *J. Phys. Chem. Lett.* **7**(12), 2258–2263 (2016). <https://doi.org/10.1021/acs.jpcclett.6b00793>
50. L. Mao, W. Ke, L. Pedesseau, Y. Wu, C. Katan et al., Hybrid Dion-Jacobson 2D lead iodide perovskites. *J. Am. Chem. Soc.* **140**(10), 3775–3783 (2018). <https://doi.org/10.1021/jacs.8b00542>
51. C.C. Stoumpos, D.H. Cao, D.J. Clark, J. Young, J.M. Rondinelli et al., Ruddlesden-Popper hybrid lead iodide perovskite 2D homologous semiconductors. *Chem. Mater.* **28**(8), 2852–2867 (2016). <https://doi.org/10.1021/acs.chemmater.6b00847>
52. Z. Tan, J. Luo, L. Yang, X. Li, Z. Deng et al., Spectrally stable ultra-pure blue perovskite light-emitting diodes boosted by square-wave alternating voltage. *Adv. Opt. Mater.* **8**(2), 1901094 (2020). <https://doi.org/10.1002/adom.201901094>
53. Y. Shen, J. Yin, B. Cai, Z. Wang, Y. Dong et al., Lead-free, stable, high-efficiency (52%) blue luminescent FA<sub>3</sub>Bi<sub>2</sub>Br<sub>9</sub>

- perovskite quantum dots. *Nanoscale Horiz.* **5**(3), 580–585 (2020). <https://doi.org/10.1039/C9NH00685K>
54. M. Shi, G. Li, W. Tian, S. Jin, X. Tao et al., Understanding the effect of crystalline structural transformation for lead-free inorganic halide perovskites. *Adv. Mater.* **32**(31), 2002137 (2020). <https://doi.org/10.1002/adma.202002137>
55. J. Pal, S. Manna, A. Mondal, S. Das, K.V. Adarsh, A. Nag, Colloidal synthesis and photophysics of  $M_3Sb_2I_9$  ( $M=Cs$  and  $Rb$ ) nanocrystals: lead-free perovskites. *Angew. Chem. Int. Ed.* **56**(45), 14187–14191 (2017). <https://doi.org/10.1002/anie.201709040>
56. A. Johnston, F. Dinic, P. Todorović, B. Chen, L.K. Sagar et al., Narrow emission from  $Rb_3Sb_2I_9$  nanoparticles. *Adv. Opt. Mater.* **8**(1), 1901606 (2020). <https://doi.org/10.1002/adom.201901606>
57. Y. Liu, Y. Zhang, Z. Yang, J. Cui, H. Wu et al., Large lead-free perovskite single crystal for high-performance coplanar x-ray imaging applications. *Adv. Opt. Mater.* **8**(19), 2000814 (2020). <https://doi.org/10.1002/adom.202000814>
58. G. Xing, B. Wu, X. Wu, M. Li, B. Du et al., Transcending the slow bimolecular recombination in lead-halide perovskites for electroluminescence. *Nat. Commun.* **8**(1), 14558 (2017). <https://doi.org/10.1038/ncomms14558>
59. J. Liu, J. Leng, K. Wu, J. Zhang, S. Jin, Observation of internal photoinduced electron and hole separation in hybrid two-dimensional perovskite films. *J. Am. Chem. Soc.* **139**(4), 1432–1435 (2017). <https://doi.org/10.1021/jacs.6b12581>
60. C. Liang, H. Gu, Y. Xia, Z. Wang, X. Liu et al., Two-dimensional Ruddlesden-Popper layered perovskite solar cells based on phase-pure thin films. *Nat. Energy* **6**(1), 38–45 (2021). <https://doi.org/10.1038/s41560-020-00721-5>
61. A.H. Proppe, R. Quintero-Bermudez, H. Tan, O. Voznyy, S.O. Kelley, E.H. Sargent, Synthetic control over quantum well width distribution and carrier migration in low-dimensional perovskite photovoltaics. *J. Am. Chem. Soc.* **140**(8), 2890–2896 (2018). <https://doi.org/10.1021/jacs.7b12551>
62. J.T. Lin, D.G. Chen, C.H. Wu, C.S. Hsu, C.Y. Chien et al., A universal approach for controllable synthesis of n-specific layered 2D perovskite nanoplates. *Angew. Chem. Int. Ed.* **60**(14), 7866–7872 (2021). <https://doi.org/10.1002/anie.202016140>
63. W. Li, C. Fang, H. Wang, S. Wang, J. Li et al., Surface depletion field in 2D perovskite microplates: structural phase transition, quantum confinement and Stark effect. *Nano Res.* **12**(11), 2858–2865 (2019). <https://doi.org/10.1007/s12274-019-2524-3>
64. Y. Gao, E. Shi, S. Deng, S.B. Shiring, J.M. Snaider et al., Molecular engineering of organic-inorganic hybrid perovskites quantum wells. *Nat. Chem.* **13**(3), 290 (2021). <https://doi.org/10.1038/s41557-020-0521-5>
65. L. Cheng, T. Jiang, Y. Cao, C. Yi, N. Wang et al., Multiple-quantum-well perovskites for high-performance light-emitting diodes. *Adv. Mater.* **32**(15), e1904163 (2020). <https://doi.org/10.1002/adma.201904163>
66. T. Chang, Q. Wei, R. Zeng, S. Cao, J. Zhao et al., Efficient energy transfer in  $Te^{4+}$ -doped  $Cs_2ZrCl_6$  vacancy-ordered perovskites and ultrahigh moisture stability via A-site Rb-alloying strategy. *J. Phys. Chem. Lett.* **12**(7), 1829–1837 (2021). <https://doi.org/10.1021/acs.jpcllett.1c00255>
67. H. Wang, X. Gong, D. Zhao, Y. Zhao, S. Wang et al., A multi-functional molecular modifier enabling efficient large-area perovskite light-emitting diodes. *Joule* **4**(9), 1977–1987 (2020). <https://doi.org/10.1016/j.joule.2020.07.002>
68. L.M. Herz, Charge-carrier dynamics in organic-inorganic metal halide perovskites. *Annu. Rev. Phys. Chem.* **67**, 65–89 (2016). <https://doi.org/10.1146/annurev-physchem-040215-112222>
69. Y.H. Kim, J.S. Kim, T.W. Lee, Strategies to improve luminescence efficiency of metal-halide perovskites and light-emitting diodes. *Adv. Mater.* **31**(47), e1804595 (2019). <https://doi.org/10.1002/adma.201804595>
70. S.D. Stranks, R. Hoyer, D. Di, R.H. Friend, F. Deschler, The physics of light emission in halide perovskite devices. *Adv. Mater.* **31**(47), e1803336 (2019). <https://doi.org/10.1002/adma.201803336>
71. X. Liu, W. Xu, S. Bai, Y. Jin, J. Wang et al., Metal halide perovskites for light-emitting diodes. *Nat. Mater.* **20**(1), 10–21 (2021). <https://doi.org/10.1038/s41563-020-0784-7>
72. Y. Jiang, M. Cui, S. Li, C. Sun, Y. Huang et al., Reducing the impact of Auger recombination in quasi-2D perovskite light-emitting diodes. *Nat. Commun.* **12**(1), 336 (2021). <https://doi.org/10.1038/s41467-020-20555-9>
73. R. Li, C. Yi, R. Ge, W. Zou, L. Cheng et al., Room-temperature electroluminescence from two-dimensional lead halide perovskites. *Appl. Phys. Lett.* **109**(15), 151101 (2016). <https://doi.org/10.1063/1.4964413>
74. X. Gong, O. Voznyy, A. Jain, W. Liu, R. Sabatini et al., Electron-phonon interaction in efficient perovskite blue emitters. *Nat. Mater.* **17**(6), 550–556 (2018). <https://doi.org/10.1038/s41563-018-0081-x>
75. D. Ma, Y. Fu, L. Dang, J. Zhai, I.A. Guzei, S. Jin, Single-crystal microplates of two-dimensional organic-inorganic lead halide layered perovskites for optoelectronics. *Nano Res.* **10**(6), 2117–2129 (2017). <https://doi.org/10.1007/s12274-016-1401-6>
76. K. Zhang, N. Zhu, M. Zhang, L. Wang, J. Xing, Opportunities and challenges in perovskite LED commercialization. *J. Mater. Chem. C* **9**(11), 3795–3799 (2021). <https://doi.org/10.1039/D1TC00232E>
77. Z. Ren, J. Yu, Z. Qin, J. Wang, J. Sun et al., High-performance blue perovskite light-emitting diodes enabled by efficient energy transfer between coupled quasi-2D perovskite layers. *Adv. Mater.* **33**(1), e2005570 (2021). <https://doi.org/10.1002/adma.202005570>
78. P. Pang, G. Jin, C. Liang, B. Wang, W. Xiang et al., Rearranging low-dimensional phase distribution of quasi-2D perovskites for efficient sky-blue perovskite light-emitting diodes. *ACS Nano* **14**(9), 11420–11430 (2020). <https://doi.org/10.1021/acsnano.0c03765>



79. Y. Shang, Y. Liao, Q. Wei, Z. Wang, B. Xiang et al., Highly stable hybrid perovskite light-emitting diodes based on Dion-Jacobson structure. *Sci. Adv.* **5**(8), w8072 (2019). <https://doi.org/10.1126/sciadv.aaw8072>
80. Y. Shi, W. Wu, H. Dong, G. Li, K. Xi et al., A strategy for architecture design of crystalline perovskite light-emitting diodes with high performance. *Adv. Mater.* **30**(25), 1800251 (2018). <https://doi.org/10.1002/adma.201800251>
81. J. Wang, N. Wang, Y. Jin, J. Si, Z. Tan et al., Interfacial control toward efficient and low-voltage perovskite light-emitting diodes. *Adv. Mater.* **27**(14), 2311–2316 (2015). <https://doi.org/10.1002/adma.201405217>
82. Z. Chen, C. Zhang, X.F. Jiang, M. Liu, R. Xia et al., High-performance color-tunable perovskite light emitting devices through structural modulation from bulk to layered film. *Adv. Mater.* (2017). <https://doi.org/10.1002/adma.201603157>
83. Z. Xiao, R.A. Kerner, L. Zhao, N.L. Tran, K.M. Lee et al., Efficient perovskite light-emitting diodes featuring nanometre-sized crystallites. *Nat. Photonics* **11**(2), 108–115 (2017). <https://doi.org/10.1038/nphoton.2016.269>
84. Z. Li, Z. Chen, Y. Yang, Q. Xue, H.L. Yip et al., Modulation of recombination zone position for quasi-two-dimensional blue perovskite light-emitting diodes with efficiency exceeding 5. *Nat. Commun.* **10**(1), 1027 (2019). <https://doi.org/10.1038/s41467-019-09011-5>
85. M. Lu, Y. Zhang, S. Wang, J. Guo, W.W. Yu et al., Metal halide perovskite light-emitting devices: Promising technology for next-generation displays. *Adv. Funct. Mater.* **29**(30), 1902008 (2019). <https://doi.org/10.1002/adfm.201902008>
86. Y. Shirasaki, G.J. Supran, W.A. Tisdale, V. Bulovic, Origin of efficiency roll-off in colloidal quantum-dot light-emitting diodes. *Phys. Rev. Lett.* **110**(21), 217403 (2013). <https://doi.org/10.1103/PhysRevLett.110.217403>
87. L. Xu, J. Li, B. Cai, J. Song, F. Zhang et al., A bilateral interfacial passivation strategy promoting efficiency and stability of perovskite quantum dot light-emitting diodes. *Nat. Commun.* **11**(1), 3902 (2020). <https://doi.org/10.1038/s41467-020-17633-3>
88. Y. Dong, Y.K. Wang, F. Yuan, A. Johnston, Y. Liu et al., Bipolar-shell resurfacing for blue LEDs based on strongly confined perovskite quantum dots. *Nat. Nanotechnol.* **15**(8), 668–674 (2020). <https://doi.org/10.1038/s41565-020-0714-5>
89. A. Fakharuddin, W. Qiu, G. Croes, A. Devižis, R. Gegevičius et al., Reduced efficiency roll-off and improved stability of mixed 2D/3D perovskite light emitting diodes by balancing charge injection. *Adv. Funct. Mater.* **29**(37), 1904101 (2019). <https://doi.org/10.1002/adfm.201904101>
90. Y. Sun, Q. Su, H. Zhang, F. Wang, S. Zhang et al., Investigation on thermally induced efficiency roll-off: toward efficient and ultrabright quantum-dot light-emitting diodes. *ACS Nano* **13**(10), 11433–11442 (2019). <https://doi.org/10.1021/acsnano.9b04879>
91. W. Zou, R. Li, S. Zhang, Y. Liu, N. Wang et al., Minimising efficiency roll-off in high-brightness perovskite light-emitting diodes. *Nat. Commun.* **9**(1), 608 (2018). <https://doi.org/10.1038/s41467-018-03049-7>
92. Z. Chen, Z. Li, C. Zhang, X.F. Jiang, D. Chen et al., Recombination dynamics study on nanostructured perovskite light-emitting devices. *Adv. Mater.* **30**(38), e1801370 (2018). <https://doi.org/10.1002/adma.201801370>
93. M. Lu, J. Guo, S. Sun, P. Lu, J. Wu et al., Bright CsPbI<sub>3</sub> perovskite quantum dot light-emitting diodes with top-emitting structure and a low efficiency roll-off realized by applying zirconium acetylacetonate surface modification. *Nano Lett.* **20**(4), 2829–2836 (2020). <https://doi.org/10.1021/acs.nanolett.0c00545>
94. M.U. Ali, J. Miao, J. Cai, D.F. Perepichka, H. Yang et al., Boosting efficiency and curtailing the efficiency roll-off in green perovskite light-emitting diodes via incorporating ytterbium as cathode interface layer. *ACS Appl. Mater. Interfaces* **12**(16), 18761–18768 (2020). <https://doi.org/10.1021/acsami.0c00950>
95. Y. Wang, Y. Teng, P. Lu, X. Shen, P. Jia et al., Low roll-off perovskite quantum dot light-emitting diodes achieved by augmenting hole mobility. *Adv. Funct. Mater.* **30**(19), 1910140 (2020). <https://doi.org/10.1002/adfm.201910140>
96. X. Zhang, C. Sun, Y. Zhang, H. Wu, C. Ji et al., Bright perovskite nanocrystal films for efficient light-emitting devices. *J. Phys. Chem. Lett.* **7**(22), 4602–4610 (2016). <https://doi.org/10.1021/acs.jpcclett.6b02073>
97. I.D. Parker, Carrier tunneling and device characteristics in polymer light-emitting diodes. *J. Appl. Phys.* **75**(3), 1656–1666 (1994). <https://doi.org/10.1063/1.356350>
98. T. Han, M. Choi, S. Woo, S. Min, C. Lee, T. Lee, Molecularly controlled interfacial layer strategy toward highly efficient simple-structured organic light-emitting diodes. *Adv. Mater.* **24**(11), 1487–1493 (2012). <https://doi.org/10.1002/adma.201104316>
99. J. Byun, H. Cho, C. Wolf, M. Jang, A. Sadhanala et al., Efficient visible quasi-2D perovskite light-emitting diodes. *Adv. Mater.* **28**(34), 7515–7520 (2016). <https://doi.org/10.1002/adma.201601369>
100. X. Zhang, W. Yin, W. Zheng, A.L. Rogach, Perovskite quantum dots with atomic crystal shells for light-emitting diodes with low efficiency roll-off. *ACS Energy Lett.* **5**(9), 2927–2934 (2020). <https://doi.org/10.1021/acsenerylett.0c01560>
101. X. Zhang, H. Lin, H. Huang, C. Reckmeier, Y. Zhang et al., Enhancing the brightness of cesium lead halide perovskite nanocrystal based green light-emitting devices through the interface engineering with perfluorinated ionomer. *Nano Lett.* **16**(2), 1415–1420 (2016). <https://doi.org/10.1021/acs.nanolett.5b04959>
102. C. Zou, Y. Liu, D.S. Ginger, L.Y. Lin, Suppressing efficiency roll-off at high current densities for ultra-bright green perovskite light-emitting diodes. *ACS Nano* **14**(5), 6076–6086 (2020). <https://doi.org/10.1021/acsnano.0c01817>
103. L.N. Quan, Y. Zhao, F.P. García De Arquer, R. Sabatini, G. Walters et al., Tailoring the energy landscape in quasi-2D halide perovskites enables efficient green-light emission. *Nano Lett.* **17**(6), 3701–3709 (2017). <https://doi.org/10.1021/acs.nanolett.7b00976>



104. V.V. Klimov, A.A. Mikhailovsky, D.W. Mcbranch, C.A. Leatherdale, M.G. Bawendi, Quantization of multiparticle Auger rates in semiconductor quantum dots. *Science* **287**(5455), 1011–1013 (2000). <https://doi.org/10.1126/science.287.5455.1011>
105. R.L. Milot, R.J. Sutton, G.E. Eperon, A.A. Haghighirad, H.J. Martinez et al., Charge-carrier dynamics in 2D hybrid metal-halide perovskites. *Nano Lett.* **16**(11), 7001–7007 (2016). <https://doi.org/10.1021/acs.nanolett.6b03114>
106. W. Xu, Q. Hu, S. Bai, C. Bao, Y. Miao et al., Rational molecular passivation for high-performance perovskite light-emitting diodes. *Nat. Photonics* **13**(6), 418–424 (2019). <https://doi.org/10.1038/s41566-019-0390-x>
107. Y. Vaynzof, The future of perovskite photovoltaics-thermal evaporation or solution processing? *Adv. Energy Mater.* **10**(48), 2003073 (2020). <https://doi.org/10.1002/aenm.202003073>
108. X. Cao, L. Zhi, Y. Jia, Y. Li, K. Zhao et al., A review of the role of solvents in formation of high-quality solution-processed perovskite films. *ACS Appl. Mater. Interfaces* **11**(8), 7639–7654 (2019). <https://doi.org/10.1021/acsami.8b16315>
109. X. Shi, Y. Liu, Z. Yuan, X. Liu, Y. Miao et al., Optical energy losses in organic-inorganic hybrid perovskite light-emitting diodes. *Adv. Opt. Mater.* **6**(17), 1800667 (2018). <https://doi.org/10.1002/adom.201800667>
110. M.M. Tavakoli, P. Yadav, D. Prochowicz, M. Sponseller, A. Osherov et al., Controllable perovskite crystallization via antisolvent technique using chloride additives for highly efficient planar perovskite solar cells. *Adv. Energy Mater.* **9**(17), 1803587 (2019). <https://doi.org/10.1002/aenm.201803587>
111. M. Abdi-Jalebi, Z. Andaji-Garmaroudi, S. Cacovich, C. Stavrakas, B. Philippe et al., Maximizing and stabilizing luminescence from halide perovskites with potassium passivation. *Nature* **555**(7697), 497–501 (2018). <https://doi.org/10.1038/nature25989>
112. S.D. Stranks, Nonradiative losses in metal halide perovskites. *ACS Energy Lett.* **2**(7), 1515–1525 (2017). <https://doi.org/10.1021/acsenerylett.7b00239>
113. S. Lee, D.B. Kim, J.C. Yu, C.H. Jang, J.H. Park et al., Versatile defect passivation methods for metal halide perovskite materials and their application to light-emitting devices. *Adv. Mater.* **31**(20), 1805244 (2018). <https://doi.org/10.1002/adma.201805244>
114. F. Yuan, X. Zheng, A. Johnston, Y. Wang, C. Zhou et al., Color-pure red light-emitting diodes based on two-dimensional lead-free perovskites. *Sci. Adv.* **6**(42), b253 (2020). <https://doi.org/10.1126/sciadv.abb0253>
115. T. Cheng, C. Qin, S. Watanabe, T. Matsushima, C. Adachi, Stoichiometry control for the tuning of grain passivation and domain distribution in green quasi-2D metal halide perovskite films and light-emitting diodes. *Adv. Funct. Mater.* **30**(24), 2001816 (2020). <https://doi.org/10.1002/adfm.202001816>
116. L. Jhuang, G. Kumar, F. Chen, Localized surface plasmon resonance of copper nanoparticles improves the performance of quasi-two-dimensional perovskite light-emitting diodes. *Dyes Pigments* **188**, 109204 (2021). <https://doi.org/10.1016/j.dyepig.2021.109204>
117. L. Zhang, C. Sun, T. He, Y. Jiang, J. Wei et al., High-performance quasi-2D perovskite light-emitting diodes: from materials to devices. *Light Sci. Appl.* (2021). <https://doi.org/10.1038/s41377-021-00501-0>
118. J. Xing, Y. Zhao, M. Askerka, L.N. Quan, X. Gong et al., Color-stable highly luminescent sky-blue perovskite light-emitting diodes. *Nat. Commun.* **9**(1), 3541 (2018). <https://doi.org/10.1038/s41467-018-05909-8>
119. D.B. Kim, S. Lee, C.H. Jang, J.H. Park, A.Y. Lee, M.H. Song, Uniform and large-area cesium-based quasi-2D perovskite light-emitting diodes using hot-casting method. *Adv. Mater. Interfaces* **7**(8), 1902158 (2020). <https://doi.org/10.1002/admi.201902158>
120. Q. Wang, X. Wang, Z. Yang, N. Zhou, Y. Deng et al., Efficient sky-blue perovskite light-emitting diodes via photoluminescence enhancement. *Nat. Commun.* **10**(1), 5633 (2019). <https://doi.org/10.1038/s41467-019-13580-w>
121. L. Zhang, T. Jiang, C. Yi, J. Wu, X. Liu et al., Bright free exciton electroluminescence from Mn-doped two-dimensional layered perovskites. *J. Phys. Chem. Lett.* **10**(11), 3171–3175 (2019). <https://doi.org/10.1021/acs.jpcclett.9b01326>
122. Z. He, Y. Liu, Z. Yang, J. Li, J. Cui et al., High-efficiency red light-emitting diodes based on multiple quantum wells of phenylbutylammonium-cesium lead iodide perovskites. *ACS Photonics* **6**(3), 587–594 (2019). <https://doi.org/10.1021/acsp Photonics.8b01435>
123. H. Tsai, C. Liu, E. Kingstein, M. Li, S. Tretiak et al., Critical role of organic spacers for bright 2D layered perovskites light-emitting diodes. *Adv. Sci.* **7**(7), 1903202 (2020). <https://doi.org/10.1002/advs.201903202>
124. M. Yu, C. Yi, N. Wang, L. Zhang, R. Zou et al., Control of barrier width in perovskite multiple quantum wells for high performance green light-emitting diodes. *Adv. Opt. Mater.* **7**(3), 1801575 (2019). <https://doi.org/10.1002/adom.201801575>
125. K. Zheng, Y. Chen, Y. Sun, J. Chen, P. Chábera et al., Interphase charge and energy transfer in Ruddlesden-Popper 2D perovskites: Critical role of the spacing cations. *J. Mater. Chem. A* **6**(15), 6244–6250 (2018). <https://doi.org/10.1039/C8TA01518J>
126. L. Zhu, D. Liu, J. Wang, N. Wang, Large organic cations in quasi-2D perovskites for high-performance light-emitting diodes. *J. Phys. Chem. Lett.* **11**(20), 8502–8510 (2020). <https://doi.org/10.1021/acs.jpcclett.0c02476>
127. J. Mao, H. Lin, F. Ye, M. Qin, J.M. Burkhartsmeyer et al., All-perovskite emission architecture for white light-emitting diodes. *ACS Nano* **12**(10), 10486–10492 (2018). <https://doi.org/10.1021/acsnano.8b06196>
128. Z. Ren, X. Xiao, R. Ma, H. Lin, K. Wang et al., Hole transport bilayer structure for quasi-2D perovskite based blue light-emitting diodes with high brightness and good spectral stability. *Adv. Funct. Mater.* **29**(43), 1905339 (2019). <https://doi.org/10.1002/adfm.201905339>



129. P. Chen, Y. Meng, M. Ahmadi, Q. Peng, C. Gao et al., Charge-transfer versus energy-transfer in quasi-2D perovskite light-emitting diodes. *Nano Energy* **50**, 615–622 (2018). <https://doi.org/10.1016/j.nanoen.2018.06.008>
130. Z. Wang, F. Wang, W. Sun, R. Ni, S. Hu et al., Manipulating the trade-off between quantum yield and electrical conductivity for high-brightness quasi-2D perovskite light-emitting diodes. *Adv. Funct. Mater.* **28**(47), 1804187 (2018). <https://doi.org/10.1002/adfm.201804187>
131. P. Vashishtha, M. Ng, S.B. Shivarudraiah, J.E. Halpert, High efficiency blue and green light-emitting diodes using Ruddlesden-Popper inorganic mixed halide perovskites with butylammonium interlayers. *Chem. Mater.* **31**(1), 83–89 (2019). <https://doi.org/10.1021/acs.chemmater.8b02999>
132. S. Lee, D.B. Kim, I. Hamilton, M. Daboczi, Y.S. Nam et al., Control of interface defects for efficient and stable quasi-2D perovskite light-emitting diodes using nickel oxide hole injection layer. *Adv. Sci.* **5**(11), 1801350 (2018). <https://doi.org/10.1002/advs.201801350>
133. Q. Zhang, M.M. Tavakoli, L. Gu, D. Zhang, L. Tang et al., Efficient metal halide perovskite light-emitting diodes with significantly improved light extraction on nanophotonic substrates. *Nat. Commun.* **10**(1), 727 (2019). <https://doi.org/10.1038/s41467-019-08561-y>
134. L. Kong, X. Zhang, Y. Li, H. Wang, Y. Jiang et al., Smoothing the energy transfer pathway in quasi-2D perovskite films using methanesulfonate leads to highly efficient light-emitting devices. *Nat. Commun.* **12**(1), 1246 (2021). <https://doi.org/10.1038/s41467-021-21522-8>
135. M. You, H. Wang, F. Cao, C. Zhang, T. Zhang et al., Improving efficiency and stability in quasi-2D perovskite light-emitting diodes by a multifunctional LiF interlayer. *ACS Appl. Mater. Interfaces* **12**(38), 43018–43023 (2020). <https://doi.org/10.1021/acsami.0c11762>
136. N. Yantara, A. Bruno, A. Iqbal, N.F. Jamaludin, C. Soci et al., Designing efficient energy funneling kinetics in Ruddlesden-Popper perovskites for high-performance light-emitting diodes. *Adv. Mater.* **30**(33), 1800818 (2018). <https://doi.org/10.1002/adma.201800818>
137. X.Y. Chin, A. Perumal, A. Bruno, N. Yantara, S.A. Veldhuis et al., Self-assembled hierarchical nanostructured perovskites enable highly efficient LEDs via an energy cascade. *Energ. Environ. Sci.* **11**(7), 1770–1778 (2018). <https://doi.org/10.1039/C8EE00293B>
138. X. Zhang, C. Wang, Y. Zhang, X. Zhang, S. Wang et al., Bright orange electroluminescence from lead-free two-dimensional perovskites. *ACS Energy Lett.* **4**(1), 242–248 (2019). <https://doi.org/10.1021/acsenenergylett.8b02239>
139. Y.F. Ng, B. Febriansyah, N.F. Jamaludin, D. Giovanni, N. Yantara et al., Design of 2D templating molecules for mixed-dimensional perovskite light-emitting diodes. *Chem. Mater.* **32**(19), 8097–8105 (2020). <https://doi.org/10.1021/acs.chemmater.0c00513>
140. P. Cai, X. Wang, H.J. Seo, X. Yan, Bluish-white-light-emitting diodes based on two-dimensional lead halide perovskite ( $C_6H_5C_2H_4NH_3$ )<sub>2</sub>PbCl<sub>2</sub>Br<sub>2</sub>. *Appl. Phys. Lett.* **112**(15), 153901 (2018). <https://doi.org/10.1063/1.5023797>
141. Z. Chu, Y. Zhao, F. Ma, C.X. Zhang, H. Deng et al., Large cation ethylammonium incorporated perovskite for efficient and spectra stable blue light-emitting diodes. *Nat. Commun.* **11**(1), 4165 (2020). <https://doi.org/10.1038/s41467-020-17943-6>
142. X. Yang, X. Zhang, J. Deng, Z. Chu, Q. Jiang et al., Efficient green light-emitting diodes based on quasi-two-dimensional composition and phase engineered perovskite with surface passivation. *Nat. Commun.* (2018). <https://doi.org/10.1038/s41467-018-02978-7>
143. Y. Jiang, C. Qin, M. Cui, T. He, K. Liu et al., Spectra stable blue perovskite light-emitting diodes. *Nat. Commun.* **10**(1), 1868 (2019). <https://doi.org/10.1038/s41467-019-09794-7>
144. J.H. Warby, B. Wenger, A.J. Ramadan, R.D.J. Oliver, H.C. Sansom et al., Revealing factors influencing the operational stability of perovskite light-emitting diodes. *ACS Nano* **14**(7), 8855–8865 (2020). <https://doi.org/10.1021/acsnano.0c03516>
145. X. Yang, Z. Chu, J. Meng, Z. Yin, X. Zhang et al., Effects of organic cations on the structure and performance of quasi-two-dimensional perovskite-based light-emitting diodes. *J. Phys. Chem. Lett.* **10**(11), 2892–2897 (2019). <https://doi.org/10.1021/acs.jpcllett.9b00910>
146. W. Deng, X. Jin, Y. Lv, X. Zhang, X. Zhang, J. Jie, 2D Ruddlesden-Popper perovskite nanoplate based deep-blue light-emitting diodes for light communication. *Adv. Funct. Mater.* **29**(40), 1903861 (2019). <https://doi.org/10.1002/adfm.201903861>
147. C. Qin, T. Matsushima, W.J. Potscavage, A.S.D. Sandanayaka, M.R. Leyden et al., Triplet management for efficient perovskite light-emitting diodes. *Nat. Photonics* **14**(2), 70–75 (2019). <https://doi.org/10.1038/s41566-019-0545-9>
148. B. Han, S. Yuan, T. Fang, F. Zhang, Z. Shi et al., Novel lewis base cyclam self-passivation of perovskites without an anti-solvent process for efficient light-emitting diodes. *ACS Appl. Mater. Interfaces* **12**(12), 14224–14232 (2020). <https://doi.org/10.1021/acsami.0c02768>
149. Y. Wang, D. Ma, F. Yuan, K. Singh, J.M. Pina et al., Chelating-agent-assisted control of CsPbBr<sub>3</sub> quantum well growth enables stable blue perovskite emitters. *Nat. Commun.* **11**(1), 3674 (2020). <https://doi.org/10.1038/s41467-020-17482-0>
150. D. Ma, P. Todorovic, S. Meshkat, M.I. Saidaminov, Y. Wang et al., Chloride insertion-immobilization enables bright, narrowband, and stable blue-emitting perovskite diodes. *J. Am. Chem. Soc.* **142**(11), 5126–5134 (2020). <https://doi.org/10.1021/jacs.9b12323>
151. J. Si, Y. Liu, Z. He, H. Du, K. Du et al., Efficient and high-color-purity light-emitting diodes based on in situ grown films of CsPbX<sub>3</sub> (X = Br, I) nanoplates with controlled thicknesses. *ACS Nano* **11**(11), 11100–11107 (2017). <https://doi.org/10.1021/acsnano.7b05191>
152. Y. Liu, J. Cui, K. Du, H. Tian, Z. He et al., Efficient blue light-emitting diodes based on quantum-confined bromide perovskite nanostructures. *Nat. Photonics* **13**(11), 760–764 (2019). <https://doi.org/10.1038/s41566-019-0505-4>

153. D. Cortecchia, W. Mróz, S. Neutzner, T. Borzda, G. Folpini et al., Defect engineering in 2D perovskite by Mn(II) doping for light-emitting applications. *Chemistry* **5**(8), 2146–2158 (2019). <https://doi.org/10.1016/j.chempr.2019.05.018>
154. J. Chang, S. Zhang, N. Wang, Y. Sun, Y. Wei et al., Enhanced performance of red perovskite light-emitting diodes through the dimensional tailoring of perovskite multiple quantum wells. *J. Phys. Chem. Lett.* **9**(4), 881–886 (2018). <https://doi.org/10.1021/acs.jpcclett.7b03417>
155. T. Wu, Y. Yang, Y. Zou, Y. Wang, C. Wu et al., Nanoplatelet modulation in 2D/3D perovskite targeting efficient light-emitting diodes. *Nanoscale* **10**(41), 19322–19329 (2018). <https://doi.org/10.1039/c8nr04896g>
156. Y.C. Kim, H.J. An, D.H. Kim, J.M. Myoung, Y.J. Heo et al., High-performance perovskite-based blue light-emitting diodes with operational stability by using organic ammonium cations as passivating agents. *Adv. Funct. Mater.* **31**(5), 2005553 (2021). <https://doi.org/10.1002/adfm.202005553>
157. Y. Liu, L.K. Ono, G. Tong, H. Zhang, Y. Qi, Two-dimensional Dion-Jacobson structure perovskites for efficient sky-blue light-emitting diodes. *ACS Energy Lett.* **6**(3), 908–914 (2021). <https://doi.org/10.1021/acsenerylett.1c00129>
158. F. Wang, Z. Wang, W. Sun, Z. Wang, Y. Bai et al., High performance quasi-2D perovskite sky-blue light-emitting diodes using a dual-ligand strategy. *Small* **16**(32), 2002940 (2020). <https://doi.org/10.1002/sml.202002940>
159. Z. Ren, L. Li, J. Yu, R. Ma, X. Xiao et al., Simultaneous low-order phase suppression and defect passivation for efficient and stable blue light-emitting diodes. *ACS Energy Lett.* **5**(8), 2569–2579 (2020). <https://doi.org/10.1021/acsenerylett.0c01015>
160. S. Zeng, S. Shi, S. Wang, Y. Xiao, Mixed-ligand engineering of quasi-2D perovskites for efficient sky-blue light-emitting diodes. *J. Mater. Chem. C* **8**(4), 1319–1325 (2020). <https://doi.org/10.1039/C9TC05590H>
161. Y. Jin, Z.K. Wang, S. Yuan, Q. Wang, C. Qin et al., Synergistic effect of dual ligands on stable blue quasi-2D perovskite light-emitting diodes. *Adv. Funct. Mater.* **30**(6), 1908339 (2019). <https://doi.org/10.1002/adfm.201908339>
162. C. Wang, D. Han, J. Wang, Y. Yang, X. Liu et al., Dimension control of in situ fabricated CsPbClBr<sub>2</sub> nanocrystal films toward efficient blue light-emitting diodes. *Nat. Commun.* **11**(1), 6428 (2020). <https://doi.org/10.1038/s41467-020-20163-7>
163. F. Zhang, B. Cai, J. Song, B. Han, B. Zhang et al., Efficient blue perovskite light-emitting diodes boosted by 2D/3D energy cascade channels. *Adv. Funct. Mater.* **30**(27), 2001732 (2020). <https://doi.org/10.1002/adfm.202001732>
164. Z. Chu, Q. Ye, Y. Zhao, F. Ma, Z. Yin et al., Perovskite light-emitting diodes with external quantum efficiency exceeding 22% via small-molecule passivation. *Adv. Mater.* **33**(18), e2007169 (2021). <https://doi.org/10.1002/adma.202007169>
165. Y. Hassan, J.H. Park, M.L. Crawford, A. Sadhanala, J. Lee et al., Ligand-engineered bandgap stability in mixed-halide perovskite LEDs. *Nature* **591**(7848), 72–77 (2021). <https://doi.org/10.1038/s41586-021-03217-8>
166. F. Yuan, C. Ran, L. Zhang, H. Dong, B. Jiao et al., A cocktail of multiple cations in inorganic halide perovskite toward efficient and highly stable blue light-emitting diodes. *ACS Energy Lett.* **5**(4), 1062–1069 (2020). <https://doi.org/10.1021/acsenerylett.9b02562>
167. M. Worku, Q. He, L. Xu, J. Hong, R.X. Yang et al., Phase control and in situ passivation of quasi-2D metal halide perovskites for spectrally stable blue light-emitting diodes. *ACS Appl. Mater. Interfaces* **12**(40), 45056–45063 (2020). <https://doi.org/10.1021/acsami.0c12451>
168. F. Zhang, X. Zhang, C. Wang, M. Sun, X. Luo et al., Chlorine distribution management for spectrally stable and efficient perovskite blue light-emitting diodes. *Nano Energy* **79**, 105486 (2021). <https://doi.org/10.1016/j.nanoen.2020.105486>
169. T. Chiba, Y. Hayashi, H. Ebe, K. Hoshi, J. Sato et al., Anion-exchange red perovskite quantum dots with ammonium iodine salts for highly efficient light-emitting devices. *Nat. Photonics* **12**(11), 681–687 (2018). <https://doi.org/10.1038/s41566-018-0260-y>
170. K. Lin, J. Xing, L.N. Quan, F. de Arquer, X. Gong et al., Perovskite light-emitting diodes with external quantum efficiency exceeding 20 per cent. *Nature* **562**(7726), 245–248 (2018). <https://doi.org/10.1038/s41586-018-0575-3>
171. C.H.A. Li, Z. Zhou, P. Vashishtha, J.E. Halpert, The future is blue (LEDs): why chemistry is the key to perovskite displays. *Chem. Mater.* **31**(16), 6003–6032 (2019). <https://doi.org/10.1021/acs.chemmater.9b01650>
172. Z. Wang, T. Cheng, F. Wang, S. Dai, Z. Tan, Morphology engineering for high-performance and multicolored perovskite light-emitting diodes with simple device structures. *Small* **12**(32), 4412–4420 (2016). <https://doi.org/10.1002/sml.201601785>
173. X. Tang, M. van den Berg, E. Gu, A. Horneber, G.J. Matt et al., Local observation of phase segregation in mixed-halide perovskite. *Nano Lett.* **18**(3), 2172–2178 (2018). <https://doi.org/10.1021/acs.nanolett.8b00505>
174. A. Sadhanala, S. Ahmad, B. Zhao, N. Giesbrecht, P.M. Pearce et al., Blue-green color tunable solution processable organolead chloride-bromide mixed halide perovskites for optoelectronic applications. *Nano Lett.* **15**(9), 6095–6101 (2015). <https://doi.org/10.1021/acs.nanolett.5b02369>
175. W. Van der Stam, J.J. Geuchies, T. Altantzis, K.H.W. Van Den Bos, J.D. Meeldijk et al., Highly emissive divalent-ion-doped colloidal CsPb<sub>1-x</sub>M<sub>x</sub>Br<sub>3</sub> perovskite nanocrystals through cation exchange. *J. Am. Chem. Soc.* **139**(11), 4087–4097 (2017). <https://doi.org/10.1021/jacs.6b13079>
176. C. Bi, S. Wang, Q. Li, S.V. Kershaw, J. Tian et al., Thermally stable Copper(II)-doped cesium lead halide perovskite quantum dots with strong blue emission. *J. Phys. Chem. Lett.* **10**(5), 943–952 (2019). <https://doi.org/10.1021/acs.jpcclett.9b00290>
177. S. Hou, M.K. Gangishetty, Q. Quan, D.N. Congreve, Efficient blue and white perovskite light-emitting diodes via



- manganese doping. *Joule* **2**(11), 2421–2433 (2018). <https://doi.org/10.1016/j.joule.2018.08.005>
178. M. Liu, G. Zhong, Y. Yin, J. Miao, K. Li et al., Aluminum-doped cesium lead bromide perovskite nanocrystals with stable blue photoluminescence used for display backlight. *Adv. Sci.* **4**(11), 1700335 (2017). <https://doi.org/10.1002/advs.201700335>
179. H. Kim, J.S. Kim, J.M. Heo, M. Pei, I.H. Park et al., Proton-transfer-induced 3D/2D hybrid perovskites suppress ion migration and reduce luminance overshoot. *Nat. Commun.* **11**(1), 3378 (2020). <https://doi.org/10.1038/s41467-020-17072-0>
180. A.A. Sutanto, R. Szostak, N. Drigo, V. Queloz, P.E. Marchezi et al., In situ analysis reveals the role of 2D perovskite in preventing thermal-induced degradation in 2D/3D perovskite interfaces. *Nano Lett.* **20**(5), 3992–3998 (2020). <https://doi.org/10.1021/acs.nanolett.0c01271>
181. J.C. Yu, D.W. Kim, D.B. Kim, E.D. Jung, J.H. Park et al., Improving the stability and performance of perovskite light-emitting diodes by thermal annealing treatment. *Adv. Mater.* **28**(32), 6906–6913 (2016). <https://doi.org/10.1002/adma.201601105>
182. A. Babayigit, A. Ethirajan, M. Muller, B. Conings, Toxicity of organometal halide perovskite solar cells. *Nat. Mater.* **15**(3), 247–251 (2016). <https://doi.org/10.1038/nmat4572>
183. H. Liang, F. Yuan, A. Johnston, C. Gao, H. Choubisa et al., High color purity lead-free perovskite light-emitting diodes via Sn stabilization. *Adv. Sci.* **7**(8), 1903213 (2020). <https://doi.org/10.1002/advs.201903213>
184. K. Wang, L. Jin, Y. Gao, A. Liang, B.P. Finkenauer et al., Lead-free organic-perovskite hybrid quantum wells for highly stable light-emitting diodes. *ACS Nano* **15**(4), 6316–6325 (2021). <https://doi.org/10.1021/acsnano.1c00872>
185. A. Singh, N. Chiu, K.M. Boopathi, Y. Lu, A. Mohapatra et al., Lead-free antimony-based light-emitting diodes through the vapor-anion-exchange method. *ACS Appl. Mater. Interfaces* **11**(38), 35088–35094 (2019). <https://doi.org/10.1021/acsami.9b10602>
186. Z. Ma, Z. Shi, D. Yang, F. Zhang, S. Li et al., Electrically-driven violet light-emitting devices based on highly stable lead-free perovskite Cs<sub>3</sub>Sb<sub>2</sub>Br<sub>9</sub> quantum dots. *ACS Energy Lett.* **5**(2), 385–394 (2020). <https://doi.org/10.1021/acsenerylett.9b02096>